Titre: Title:	A study of high resolution seismic reflection lines 29-3 and 93A in the Matagami area, Abitibi Belt, Québec
Auteur: Author:	Yexu Li
Date:	1996
Type:	Mémoire ou thèse / Dissertation or Thesis
Référence: Citation:	Li, Y. (1996). A study of high resolution seismic reflection lines 29-3 and 93A in the Matagami area, Abitibi Belt, Québec [Mémoire de maîtrise, École Polytechnique de Montréal]. PolyPublie. https://publications.polymtl.ca/31084/

URL de PolyPublie: PolyPublie URL:	https://publications.polymtl.ca/31084/
Directeurs de recherche: Advisors:	Michel C. Chouteau, & Alain Calvert
Programme: Program:	Non spécifié

UNIVERSITÉ DE MONTRÉAL

A STUDY OF HIGH RESOLUTION SEISMIC REFLECTION LINES 29-3 AND 93A IN THE MATAGAMI AREA, ABITIBI BELT, QUEBEC

Yexu LI

DEPARTMENT DE GÉNIE MINÉRAL

ÉCOLE POLYTECHNIQUE DE MONTRÉAL

MÉMOIRE PRÉSENTÉ EN VUE DE L'OBTENTION

DU DIPLÔME DE MAÎTRISE ÈS SCIENCES APPLIQUÉES

(GÉNIE MINÉRAL)

JUIN 1996

UNIVERSITÉ DE MONTRÉAL

ÉCOLE POLYTECHNIQUE DE MONTRÉAL

Ce mémoire intitulé:

A STUDY OF HIGH RESOLUTION SEISMIC REFLECTION LINES 29-3 AND 93A IN THE MATAGAMI AREA, ABITIBI BELT, QUEBEC

présenté par: Yexu LI

en vue de l'obtention du diplôme de: Maîtrise ès sciences appliquées

a été dûment accepté par le jury d'examen constitué de:

M. BROWN, Alex, Ph.D., président

M. CHOUTEAU, Michel, Ph.D., membre et directeur de recherche

M. CALVERT, Andrew, Ph.D., membre et codirectur de recherche

M. WHITE, Don, Ph.D., membre

to my family

ACKNOWLEDGEMENTS

I would express my special gratitude to Marianne Mareschal, my ex-supervisor, for her encouragement of my study in Geophysics during that difficult time. I would like to extend my sincere thanks to Dr. Andrew Calvert, my co-supervisor, for his patience, advice and valuable technical recommendations. Without his knowledge and experience, this thesis would not have been possible. In particular, I wish to thank Professor Michel Chouteau, who became my new supervisor after Marianne Mareschal passed away, for allowing me complete this work. I also thank Professor Alex Brown, Dr. Don White and Dr. Dean Livelybrooks for their comprehensive review and useful comments on the manuscript of my thesis. Special thanks to Estelle Blais and Gilles Bellefleur, who performed the excellent French translation. I extend my deepest appreciation to my husband, Linag Ma, for his everlasting encouragement and moral support. Special thanks also are due to my mother for taking care of my son for the past two years. Finally, I would like to thank all of the enthusiastic and helpful friends in the department for making the past two years cherishable and memorable.

RÉSUMÉ

Dans le cadre du projet LITHOPROBE, deux profils de sismique réflexion à haute-résolution ont été acquis sur le flanc sud de l'anticlinal de Matagami, situé dans le camp minier de Matagami. Le profil 29-3 d'une longueur de 8.72 km et d'orientation E-O et le profil 93-A d'une longueur de 8 km et d'orientation N-S permettent de bien imager les diverses lithologies situées sur le flanc sud de l'anticlinal. Parmi celles-ci, on retrouve les laves mafiques du Groupe de Wabassee et les laves felsiques du Groupe de Watson Lake. Un horizon de tuf cherteux appelé "Key Tuffite", situé au contact de ces deux groupes, contient la plupart des gisements du camp minier.

La séquence de traitement des données sismiques, semblable pour les deux profils, comprend la définition de la géométrie de la ligne moyenne (slalom line), la mise à zéro des premières arrivées et l'atténuation des ondes S réfractées. Les corrections statiques de réfraction ont amélioré de façon significative les sections sismiques. Les corrections pour les pendages latéraux ont aussi amélioré les sections sommées. Les corrections statiques résiduelles ont contribué au rehaussement des réflexions situées près de la surface, tandis que la migration partielle avant sommation (DMO) a permis de résoudre les ambiguïtés sur le choix des vitesses de corrections dynamiques en présence de structures complexes.

L'interprétation de ces données est basée sur les sections migrées des profils 29-3 et 93A, de

même que sur l'information provenant de deux trous de forage situés à proximité des profils sismiques. Sur ces sections, une séquence d'excellente réflectivité étendue sur 120 ms d'enregistrement est associée à une suite interstratifiée de 400-600 m d'épaisseur constituée de gabbro, basalte, rhyolite et tuffite. Cette suite est située à la base du Groupe de Wabassee. Le Groupe de Watson Lake est essentiellement nonréflecteur. Le profil sismique 29-3 permet aussi d'identifier en profondeur le prolongement d'une faille orientée SE-NO (la faille Daniel) et d'estimer son déplacement vertical à environ 600 m.

Un levé de VSP(vertical seismic profile) a aussi été effectué dans la région du camp minier. Cependant, la forme variable des premières arrivées ne permet pas d'obtenir des réflexions de bonne qualité.

ABSTRACT

As part of the LITHOPROBE project, two high-frequency vibroseis seismic profiles, the 8.72 km-long Line 29-3 in an east-west direction and the 8 km-long Line 93A in a north-south direction, were shot across the Matagami mining camp located on the southern part of the Matagami anticlinorium. In the mining camp, most ore bodies are located at the Key Tuffite horizon, which is the contact between the mafic Wabassee Group and the underlying felsic Watson Lake Group.

The data processing was similar for both seismic profiles and includes crooked-line geometry, first-break muting and shear-wave removal. Refraction statics corrections were the most important part of the reprocessing sequence and produced the biggest improvement in the seismic image. Crossdip corrections were also an important step towards obtaining a high quality stack of Line 29-3. Accurate surface consistent residual statics correction enhanced shallow reflections and DMO(dip moveout) processing was applied to image conflicting dips.

The interpretation of the mining camp is based on both the migrated stacked sections and two available borehole log data sets available in the area. On the stacked sections of both Line 29-3 and Line 93a, a 120 ms thick strong reflective package is observed. It is believed that this reflective sequence is associated with a 400-600 m thick sequence of interlayered gabbro, basalt, ryholite and tuffite at the base of the Wabassee Group. The Watson Lake Group

appears largely non-reflective. The seismic section of line 29-3 also provides information relative to the structural geology of the volcanic complex: a deep SE-NW fault (the Daniel fault) is observed clearly and its vertical displacement is estimated to be about 600 m.

A VSP(vertical seismic profile) survey was also conducted in the vicinity of the mining camp. However, the reflections are too weak to see clearly because of the variability in the first break waveform.

CONDENSÉ EN FRANÇAIS

La **méthode de sismique réflexion** est de loin l'une des méthodes géophysiques les plus utilisées. Sa prédominance est due à sa grande exactitude, sa haute résolution et sa grande profondeur de pénétration. Les données sismiques sont utilisées pour identifier les lithologies, pour détecter les hydrocarbones et surtout le pétrole. Les données sismiques sont aussi utilisées lors de levés hydrogéologiques et en génie civil. Récemment, les données sismiques ont été utilisées dans l'exploration minière.

La base de la théorie sur laquelle la méthode de sismique réflexion est basée est la propagation des ondes élastiques. L'acquisition des données sismiques, leur traitement et leur interprétation sont trois étapes importants d'un levé sismique. Pour l'acquisition de données terrestres, la couverture multiple est la technique la plus utilisée. Le traitement des données peut être séparé en trois étapes principales: la déconvolution, la sommation des traces et la migration. La déconvolution retire l'ondelette sismique correspondant à la source des enregistrements. Elle améliore la résolution temporelle des données. La sommation ("stacking") avec point-miroir commun (CMP) somme l'énergie réfléchie du même point sous la surface, ce qui atténue le bruit non corrélé, augmentant de ce fait le rapport signal sur bruit. La migration ramène vers leur origine les diffractions et déplace les événement inclinés vers leur "position" réelle sous la surface. Donc, elle améliore la résolution spatiale. De plus, plusieurs autres traitements, tels que les corrections statiques à

partir des ondes réfractées, les corrections de pendage latéraux ("crossdip") et le DMO ("Dip Moveout"), sont nécessaires pour améliorer l'efficacité des trois étapes principales du traitement.

Finalement, l'interprétation sismique consiste à déterminer la signification géologique des données sismiques. L'interprétation des données de sismique réflexion inclue généralement la réduction des données, la sélection des événements qu'on considère comme des réflexions primaires et la déduction de leur signification. Une bonne interprétation doit être consistante plutôt que correcte.

Le **profilage sismique vertical** (VSP) est une méthode de mesure dans laquelle un signal sismique est généré à la surface de la terre et est enregistré par des géophones placés à des profondeurs différentes dans un forage. La technique VSP est une des méthodes les plus exactes pour déterminer la vitesse sismique. La principale différence entré le traitement des données VSP et celui des données de sismique réflexion traditionnelle est la séparation des ondes remontantes (ondes de réflexion) des ondes descendantes (ondes directes). Plusieurs méthodes numériques peuvent être utilisées à cet effet.

L'acquisition des données VSP de Matagami s'est faite avec une source (explosion) à la surface enregistrée par des géophones dans un forage. Un géophone près de la source a été utilisé pour déterminer le temps de détonation, afin de corriger les données enregistrées

dans le forage au temps réel. Les données ont été enregistrées par trois géophones orthogonaux (X,Y,Z) à chaque niveau de profondeur (tableau 2.1). Le traitement des données VSP inclut: (1) la correction du temps pour s'assurer que la différence entre le temps du début de l'enregistrement et le temps de détonation est la même pour tous les géophones; (2) l'analyse du bruit pour enlever le bruit généré par les camps miniers actifs; (3) la séparation des ondes descendantes et remontantes pour obtenir l'information de réflexion utile. Des filtres médians et f-k ont été utilisés à cet effet. Cependant, les ondes remontantes sont si faibles que les ondes descendantes sont encore très fortes dans la section finale.

Les lignes de sismique réflexion 29-3 et 93A. Le complexe volcanique felsique de Matagami fait partie de la ceinture de l'Abitibi, la plus grande terrane de roches vertes sur la Terre. La région de Matagami compte l'un des camps miniers de métaux de base les plus productifs au Canada. Dans le cadre du projet Lithoprobe, deux profils de sismique réflexion haute fréquence de 8.72 km et de 8 km ont été enregistrés selon une direction est-ouest et nord-sud, respectivement, dans la partie sud du camp minier. Le traitement des données pour ces deux lignes avait été précédemment choisi. Le retraitement de ces deux lignes de sismique réflexion a été fait afin de mieux comprendre la région. L'acquisition, le retraitement et l'interprétation des lignes 29-3 et 93A sont le sujet principal de ce mémoire.

Acquisition des données: Les données des deux lignes ont été recueillies en utilisant une source vibroseis et un système de télémétrie à plusieurs canaux qui comprenait la sommation sur le terrain, le rejet du bruit et des capacités de corrélation. La configuration des récepteurs employait 240 groupes de géophones placés tous les 20 m, résultant en une couverture nominale ("fold") de 120, avec un offset proche de 0 m et un offset lointain de 2400 m. Les données ont été enregistrées avec une durée de 4 s pour la ligne 29-3 et de 16 s pour la ligne 93A. Le taux d'échantillonnage est de 2 ms pour les deux lignes (tableaux 3.1 et 3.2).

Retraitement des données: Le retraitement des lignes 29-3 et 93A (tableaux 3.4 et 3.5) inclus la définition de la géométrie, la suppression du signal avant la première arrivée et l'enlèvement des ondes de cisaillement. Puisque la ligne 29-3 n'est pas droite, trois lignes slalom dans différentes directions ont été conçues. Les largeurs CDPBIN ont été choisies pour couvrir les CDP presque complètement de telle sorte qu'une couverture nominale de 100 CDP est obtenue. Les premières arrivées ont été piquées pour chaque tir après la suppression du bruit de 45, 60 et 120 Hz. Pour enlever les première arrivées et les ondes de cisaillement, je les ai premièrement alignées avec les points piqués (pour les premières arrivées) ou les vitesses (pour les ondes S); j'ai ensuite aplati les données à 0.3 ms et les ai lissées; un filtre médian a ensuite été appliqué; finalement, j'ai soustrait les données sur lesquelles le filtre médian a été appliquées des données non filtrées.

Les corrections statiques à l'aides des ondes réfractées ont été la partie la plus importante de la séquence de retraitement et on produit la plus grande amélioration des images sismiques pour les deux lignes. La technique utilisée pour ces corrections est le GLI3D, qui est basé sur la théorie de l'inversion linéaire généralisée. Un niveau de référence pour l'élévation de 300 m, une vitesse du matériel érodé de 900 m/s et une vitesse de remplacement de 6000 m/s ont été utilisées. Les corrections statiques à l'aide des ondes réfractées pour les récepteurs et les sources de la ligne 29-3 vont de -98.0 à -2.0 ms, tandis que ces corrections atteignent un maximum de -70 ms pour la ligne 93A.

Puisque la ligne 29-3 n'est pas droite, les corrections de pendage apparent ont aussi été une étape importante dans l'obtention d'une section somme de haute qualité. L'équation(3.2) a eté utiliseé pour la correction de pendage apparent. La ligne a été séparée en trois lignes effectives dont les lignes slalom étaient droites pour l'analyse de pendage apparent. Pour chacune des trois lignes, j'ai calculé la distance de pendage apparent des traces (Y_i) dans un CDP de la ligne slalom et mis la valeur dans l'entête 19. Les meilleures valeurs de D_k (tableau 3.3) pour chaque interface ont été trouvées. Des corrections de temps correspondant à l'équation (3.2) ont alors été appliquées. Après les corrections de pendage apparent, la section somme de la ligne 29-3 montrait une nette amélioration, tout particulièrement pour les événement inclinés est-ouest entre 0.75 et 1.25 s sous les CDPs 4500 à 1800 (figure 3.14).

Des corrections statiques résiduelles exactes ont été nécessaires pour faire ressortir les réflexions peu profondes des deux lignes. Le module utilisé ici pour les statiques résiduelles est Superfold, basé sur l'algorithme Ronen-Claerbout. L'idée maîtresse derrière cet algorithme est que les décalages statiques sont déterminés de telle sorte que la puissance de la section somme finale est maximisée. Pour la ligne 29-3, deux fenêtres de temps ont été appliquées séparément: premièrement, les corrections statiques résiduelles ont été appliquées dans un intervalle de 0.05 à 0.55 s, puis sur un intervalle de 0.5 à 1.5 s. Les deux fenêtres ont produit une bonne convergence après 5 itérations. Les décalages totaux maximaux étaient de 40 ms. Pour la ligne 93A, les fenêtres de temps étaient de 0.05 à 1.9 s et de 0.05 à 0.6 s. Elles ont aussi nécessité 5 itérations et les décalages totaux maximaux étaient aussi de 40 ms.

Les corrections DMO ("dip moveout") ont été utilisées pour résoudre des problèmes de pendage conflictuels. Le DMO peut être considéré comme un procédé de migration partielle. Les deux lignes 29-3 et 93A contiennent plusieurs événements inclinés. Avec le traitement sismique conventionnel, ces événements sont atténués lors de la sommation. Pour surmonter cette difficulté, le DMO est nécessaire. Une vitesse moyenne de 6000 m/s a été utilisée pour les corrections dynamiques avant le DMO. La figure 3.17 montre bien les effets du DMO sur la ligne 93A.

Une fonction de vitesse précise est critique pour obtenir une section somme finale de bonne qualité. La technique d'analyse à vitesse constante (CVA) a été utilisée pour l'analyse de vitesse des deux lignes. L'idée maîtresse de la méthode CVA est que les vitesses de sommation sont évaluées d'après les données sommées avec un choix de vitesses constantes en considérant l'amplitude des événements sommés et leur continuité. On doit se rappeler que les vitesses obtenues par la méthode CVA sont les meilleures vitesses de sommation, mais elles ne sont probablement pas les vitesses réelles de la terre. Pour les lignes 29-3 et 93A, un groupe de 20 CMPs des choisi pour le panneau de test et on analyse ainsi les vitesses à tous les 80 CMPs. Un total d'environ 10 fonctions de vitesses de groupe a été obtenu pour chaque ligne.

Finalement, la migration a été appliquée sur chaque ligne pour déplacer les réflecteurs vers leur "position" réelle sous la surface. La migration dans le domaine fréquentiel (f-k) a été utilisée. Les avantages de cette méthode sont notamment un temps de calcul rapide et une excellent performance pour les forts pendages. La théorie de la migration f-k est basée sur des techniques géométriques directes et des observations simples dans le domaine fréquentiel. Une simple migration lissée avec une vitesse de 6000 m/s a donné de bon résultats pour les deux lignes. Après la migration f-k, une analyse précise des vitesses apparentes a été appliquées pour obtenir les vitesses réelles de la terre.

Interprétation: La figure 3.22 montre la section interprétée de la ligne 29-3. Deux forages situés dans la portion est de la ligne permettait un bon contrôle stratigraphique pour l'interprétation. (1) La partie est de la ligne sismique, entre les CDP 950 et 2700, est caractérisée par une séquence de fortes réflexions inclinées vers l'ouest, sous une zone transparente. La séquence réflective provient probablement de basaltes, de gabbros et de tuffite alternées. Elle définit clairement le Groupe Wabanassee inférieur. Les réflecteurs individuels à l'intérieur de la séquence réflective sont difficiles à identifier. Le Groupe Wabanasse supérieur au-dessus semble non-réflectil. La tuffite Key et le Groupe du Lac Watson sous-jacent sont caractérisés par une faible réflectivité et peuvent être identifiés à la base du Groupe Wabassee inférieur. Le Groupe du lac Watson semble lui aussi nonréflectif sauf pour l'anomalie d'amplitude sismique "C" à environ 0.4 s de temps d'aller-retour (TWT), soit 1200 m de profondeur, sous les CDP 1850 à 2350. (2) La faille de Daniel (DF) passe sous le CDP 2900. La DF coupe les réflexions de pendage ouest atour des CDP 2800 à 2900. Le déplacement du Groupe Wabassee inférieur entre les côtés est et ouest de la DF est d'environ 0.2 s TWT, i.e. 600 m. La DF n'est probablement pas une faille isolée mais plutôt une zone complexe d'après l'image sismique. (3) La partie ouest de la ligne 29-3 (CDPs 3000 à 5300) est dominée par les fortes réflexions associées au Groupe Wabassee inférieur. Aucun forage ne permet de le vérifier. Le "paquet réflectif" peut être suivi jusqu'à une profondeur de 3 km (1.0 s TWT) à l'extrémité du profil. L'épaisseur du Groupe de Wabassee inférieur dans cette portion du profil est d'environ 900 m. (4) Il n'y a qu'une réflexion majeure de pendage est-ouest (AB)

sur cette section sismique. Elle est située sous les CDPs 2900 à 5200 entre 0.75 et 1.1 s TWT. (5) Puisque la ligne sismique change de direction à cet endroit, la nouvelle méthode de traitement rend les réflexions sous les CDPs 2700 à 2800 plus continus.

Une interprétation du profil sismique 93A est présentée à la figure 3.25. (1) Des réflexions de pendage sud peuvent être suivies de l'extrémité sud jusqu'au CDP 2700 au sud de la section. Les lignes 29-3 et 93A se croisent à la station 392 (CDP 3920) de la ligne 93A , et à la station 220 (CDP 2200) de la ligne 29-3 (Figure 3.26). À ce point, un paquet de réflexions d'une épaisseur d'environ 0.12 s peut être identifié entre 0.15 et 0.27 s TWT sur les deux lignes. Il y a de fortes réflexions sous les CDP 3000 à 4700 entre 0.27 et 0.43 s. Elles proviennent du Groupe du Lac Watson. (3) Les réflexions provenant du Groupe Wabassee inférieur et du Groupe du Lac Watson ont un pendage d'environ 30° vers le sud de la ligne 93A. Il n'y a pas d'interruption majeure dans la continuité de ces réflexions. Quelques petites cassures sont cependant visibles près de la surface sous les CDP 4300 à 4900, probablement causées par la suppression des premières arrivées. (4) La faille de Daniel devrait produire des réflexions de pendage nord sur la ligne 93A, mais on ne peut les voir clairement. Les réflexions de pendage sud augmentent sous les CDP 3000 à 4200. Il y a de fortes réflexions sous le CDP 3800 à environ 1.75 s.

Le succès de l'interprétation de deux profils de sismique réflexion haute résolution nous apporte une évidence de l'utilité des méthodes sismiques dans l'exploration minérale.

TABLE OF CONTENTS

PAGE

LIST OF FIGURES

LIST OF TABLES

CHAPTER 1

INTRODUCTION TO SEISMIC REFLECTION METHOD

1.1 Introduction

The seismic reflection method is by far one of the most widely used geophysical techniques. Its dominance is due to its high accuracy, high resolution and great penetration. Seismic data have been used for identifying lithology, generally from velocity and attenuation characteristics of the transmitted and reflected seismic waves, and for detecting hydrocarbons, primarily gas, directly on the basis of reflection amplitudes and other seismic indicators. Seismic data have also been used in groundwater surveys and in civil engineering, especially to measure the depth to bedrock in connection with the construction of large buildings, dams, and highways. Recently, seismic data have found some application in the exploration for minerals.

The basic theory on which the seismic reflection method depends is elastic wave propagation: generating seismic waves using a near-surface explosion, mechanical impact, or vibrations and measuring the times required for a seismic wave (or pulse) to return to the surface after reflection from interfaces between sub-surface having different physical properties. Lateral variations in the reflection time of a horizon on the seismic section usually indicate a structural feature in the strata below. Depths to the reflective structures can be estimated from the recorded reflection times. Velocities of the rocks can be obtained from reflected seismic data themselves or surveys in wells.

Recent technological improvements in seismic data acquisition and processing have made it possible to obtain usable reflection data in many areas where reflections were formerly too poor to map. However, there remain places where the seismic reflection method still does not yield a reliable interpretation and in such cases, other geophysical methods must be employed.

1.2 Seismic Reflection Data Acquisition

There are several different ways to acquire land and marine data. To acquire quality data, a seismic line must be designed properly: data migration may require that lines be located other than directly on top of the objective; near-surface variations may be so large that the data are difficult to interpret, whereas moving the seismic line a short distance may improve data quality.

In land data acquisition, multiple-channel recording is needed to distinguish reflections from ground motion due to other sources (noise). A seismic cable is laid on the ground with provision for connecting groups of geophones at regular intervals. Each group transmits its data to the recording instruments on one information channel. With such an arrangement, each shot yields information on the structure of a subsurface interface at a large number of reflecting points distributed along the line.

Multifold coverage is another important technique for land data acquisition, i.e. CMP

profiling or roll-along shooting. For example, in figure 1.1, 24 geophone groups are evenly spaced and are connected to the amplifier inputs in the recording truck. Then shot A, B, C, D, E, F are fired sequentially. Seismic data are recorded for each shot. During post-survey data processing, the data are sorted to CMP gather and normal-moveout corrected using a stacking velocity. The traces are then stacked to enhance the signal-to-noise ratio of the subsurface signals.

There are different spread types: end-on spread, in-line offset spread, broadside-T spread, cross-spreads and so on.

1.3 Seismic Data Processing

The quality of a seismic profile depends mainly on two aspects: the field acquisition parameters and the tools used for processing. Seismic data processing can be viewed as comprising three principal processes: deconvolution, stacking, and migration. Deconvolution removes the basic seismic wavelet (source function) from the recorded traces by collapsing the seismic wavelet approximately to a spike and suppressing reverberations on the field data. Hence, it improves temporal resolution. Deconvolution techniques are often based on optimum Wiener filtering.

Common-midpoint (CMP) stacking is the most important step of the three principal groups

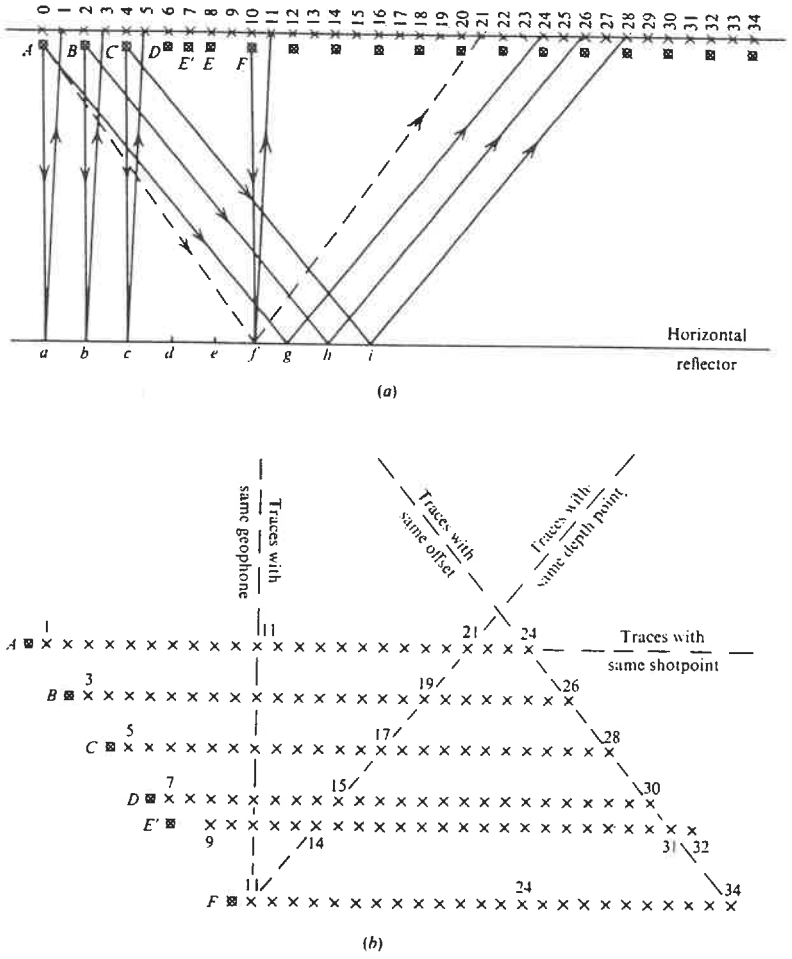

Figure 1.1 CDP profiles. The symbols x and O represent geophone groups and shotpoints respectively. (a) Vertical illustrating CDP shooting; (b) CDP stacking chart (modified after Telford, 1976).

of processes. In Figure 1.1, assuming a horizontal reflector, shot A is fired into geophones from a to g. Shot B gives sub-surface coverage from b to h, and so on down to the seismic line. The reflection point for the energy from shot A into geophone group 21 is point f, which is also the reflecting point for the energy from B into geophone group 19, from C into 17, from D into 15, from E into 13 and from F into 11. This is a so called CMP(common mid-point) gather. A "normal moveout correction(NMO)" is then applied to the CMP gather so that the reflection hyperbolas are straightened out, after which the six traces are summed to give one trace in the final stack corresponding to the depth point f. CMP stacking can significantly suppress uncorrelated noise, thereby increasing the S/N ratio.

Finally, migration collapses diffractions and moves dipping events to their true subsurface location. It is commonly applied to stacked data. Migration is usually based on the wave equation and improves spatial resolution. When the stacked section is not properly migrated, it can often be traced to the imprecision of the velocity information available for the input to the migration program.

Many other processes are required to improve the effectiveness of the three primary processes. For example, refraction statics are required in land data to remove the deviation in travel times from regular hyperbolic moveout, and thus improve the quality of stack. Bandpass filtering may also be needed to remove very low- and high-frequency noise so that the S/N ratio is increased. Crossdip correction may also be an important step prior to the

stacking of crooked lines. Velocity analysis, which is an essential step for stacking, can be improved by multiple suppression and residual statics corrections.

1.4 Seismic Reflection Interpretation

Seismic interpretation involves determining the geologic significance of seismic data. The reflection interpretation generally includes data reduction, selecting events believed to be primary reflections and deducing their significance. The test of a good interpretation is consistency rather than correctness. Not only must an interpretation be consistent with all the seismic data, but it also must be consistent with all that is known about the area, including gravity and magnetic data, well information and surface geology, as well as geologic and physical concepts (Sheriff, 1982).

The basic seismic reflection interpretation techniques include:

1. Mapping reflection horizons: Reflections are usually identified with bedding planes based on correlations with observations in boreholes, velocity information, synthetic seismograms or previous experience in the area. The horizons which are drawn on seismic sections provide two-dimensional pictures only. To obtain three-dimensional information, lines acquired in different directions in the same area are necessary. Events picked on one seismic line are compared with those on intersecting profiles in order to identify the same horizons.

Correction is made on the basis of character and arrival times.

2. Geologic structure style: Some geologic structures, such as anticlines, faults, unconformities etc. are usually evident from examination of the seismic reflection section maps. But some structures, such as pinchouts, are more difficult to recognize and nonseismic evidence (such as gravity field mapping) must often be combined with seismic data to identify such features.

(a) *Faulting*: Ideally, reflection events terminate sharply as the point of reflection reaches the fault plane and then they resume again in displaced positions on the other side of the fault. Moreover, a reflection often has a sufficiently distinctive character that the two portions on opposite sides of the fault can be recognized and the throw of the fault determined. In practice, diffractions usually prolong events on unmigrated sections so that the location of the fault plane is not clearly evident. Sometimes the same reflection can be identified unequivocally on the two sides of a fault, but in most cases we can make tentative correlations. Campbell (1965) discussed criteria for detecting faults on a seismic section for such a situation. Another feature that is often observed from a seismic section is distortion of events whose raypaths passed through the fault plane and experienced bending at the fault plane. This effect results from local velocity changes at the faults. In fact, the distortion may be so great and may change so rapidly as to cause a marked deterioration of data quality below the fault. This effect can sometimes be so great that reflections are entirely absent ("a

shadow zone"). The type of fault (normal fault, thrust fault etc.) can usually be determined by the dip of the fault and the offset of stratigraphy on the seismic section.

(b) *Fold and flow structures*: When subject to stress, rocks may fault, fold or flow, depending on the magnitude and duration of the stresses, the strength of the rocks, etc. On a seismic section, anticlinal curvature tends to make seismic reflections weaker as well as increase the likelihood of faulting and flow, so that data quality commonly deteriorates over anticlines. Salt flow often produces salt domes, which usually can be seen clearly on a seismic section because the top of the salt dome is strongly reflective. Defining the flank of a saltdome precisely is often important economically, but at the same time, it is difficult seismically. Fortunately, the velocity distribution is often only slightly affected by the development of the dome so that the steep dips of the sediments adjacent to the flanks can be migrated fairly accurately and the flank outlined by the terminations of these reflections.

(c) *Reefs:* There are wide variety of reefs, including both extensive barrier reefs which cover large areas and small isolated pinnacle reefs. Reefs are carbonate structures built directly by organisms, aggregates comprising limestone and other related carbonate rocks. The evidence for reefs is often so subtle that seismic mapping is feasible only in areas of well documented geology.

(d) *Unconformities and channels*: Unconformities represent a missing rock unit. Usually

unconformities are good reflectors because there is a big velocity and density difference between two different geologic units. On a seismic section, these reflectors are the easiest to be recognized.

3. Deducing geological history: After the structural information has been extracted, the next step is to work out the geologic history of an area. Seismic sections often subdivide into units. The boundaries between units are often the better reflectors and the units have angular relations to each other which indicate different stages of history: tectonic activity, development of unconformities, marine transgressions, etc. The boundaries between units generally indicate a period of geologic time and often separate sediments deposited in different kinds of environments. Velocity and other seismic measurements, such as amplitude or instantaneous frequency, yield additional information.

4. Integrating well data into an interpretation: Wells drilled in an area provide geologic information which must be consistent with the interpretation of a seismic line. Borehole logs are interpreted to determine formation tops, lithology, depositional environment, the location of faults and unconformities with an indication of the amount of section missing, etc. Well log information is usually plotted linearly in time at the seismic section scale in order to help the interpretation. However, for several reasons, such as the locations of wells being away from the seismic line, relating interfaces to specific seismic events is not always easy.

5. Drawing conclusions from reflection data and other geophysical data: A final interpretation of a seismic line should be made by utilizing all available data. Gravity and magnetic data should be examined to see if they are consistent with the mapped features. Refraction velocities may help in identification of the nature of certain reflectors, especially where seismic record quality is poor. Magnetotelluric soundings may be useful in reducing interpretation ambiguities.

CHAPTER 2

VERTICAL SEISMIC PROFILING

2.1 Introduction

The most accurate methods of determining seismic velocity are borehole surveys. The vertical seismic profile (VSP) is one type of well survey. The conventional borehole survey involves placing a geophone at different depths and measuring the traveltime of the first energy (first break) from a near wellhead source. The geometry for VSP is similar except that the entire wavetrain is recorded (Hardage, 1985). This implies that the wavetrains include direct waves, reflections and multiples of various types. Thus, VSP records are not only used for determining velocities, but also, are more useful in recording reflections from subsurface boundaries, such as faults that are not clear in surface-recorded data. VSP records usually have greater bandwidth than surface data because the waves have not had as far to travel.

In a VSP survey, the geophones are usually located in different depths and closely spaced in wells (about 25 m). In offset VSPs, the source is placed some distance from the wellhead so that the reflecting points will be located further from the well, i.e. the further reflecting horizons from the well can be recorded. In all type of VSP, the recorded wavetrains typically contain downgoing and upgoing waves. The downgoing modes contain direct waves, and they provide the information needed for deconvolution of the upgoing wavefield. The upgoing modes include the predominately primary reflections and are useful in correlating reflection events with other data. The main data processing for VSP data is the separation of the downgoing and upgoing waves.

2.2 Data Acquisition

The VSP data in Bell Allard South (figure 3.1) area were collected in 1994 by Noranda Inc. The length of the well is 4396.00 feet (1340.78 m), along an azimuth approximately 202°28'; maximum deviation is around 10°. The data acquisition involved a surface source (shot), recorded by a downhole geophone. The shot was located around 300 m away from the well head, and was in roughly the same vertical plane as the well. The near-shot geophone was used to determine the shot detonation time, in order to correct to the recorded downhole data to the true time. The data were recorded by three orthogonal geophones (X, Y, Z) at each

Table 2.1: Data Acquisition Parameters for VSP:

WELL	
Well Length	1340.78 m
Well Orientation	202°28'
Well Slope	84°35'
SOURCE	
Source Type	Dynamite
Distance from Well Head	300 m
GEOPHONE	
Geophone Type	14 Hz natural frequency
Geophone Spacing	10 m
RECORDING	
Record length	0.6 s
Sampling	0.1 ms
Total records	120

depth level. Then, the geophone was moved to a new depth level and the recording was repeated. The distance between depth levels was about 10 m, and in totally 120 levels were

recorded. The data were recorded for 0.6 s and at a sample interval of 0.1 ms. Table 2.1 presents the basic parameters of the data acquisition.

2.3 Data Processing

Several problems become apparent when unprocessed VSP data are used for interpretation. The first and main problem is that the downgoing wavefield is so dominant that any interpretation of the upgoing primary reflections is difficult and often impossible. In addition, both random and coherent noise contaminate the data, source wavelets are longer than desired, and numerous surface and interbed multiples exist. Therefore, data processing is required to achieve the maximum utilization of VSP field data, particularly if interpretation of the upgoing primary reflection events is required.

The procedures are designed depending on different VSP data and the desired applications. Much of processing is similar to that for conventional surface seismic reflection data. Several numerical techniques can be used to emphasize upgoing reflection: vertical summation, velocity filtering, deconvolution, etc..

For the Matagami VSP data, the data processing includes: time correction, noise reduction, and downgoing and upgoing separation.

2.3.1 Time Correction:

The recording system in this survey cannot assure that the differences between start-recording time and shot-time for all geophones are the same, i.e.: the data can not be displayed as one shot gather. To obtain a one-shot-gather section for all of the recordings, a time correction is needed before any data processing. The surface recordings are used for this purpose.

Displaying the surface recordings, the first breaks are not aligned. A time shift is applied on each trace so that every first-break moves to the average first-break time. Then the same time shift is applied to the downhole data for each trace so that the downhole data act as one shot gather although they are recorded with different shots.

Following the time correction, the traces were edited. The 205th, 260th and 301th traces were removed because they are dominated by noise.

2.3.2 Noise

Numerous sources of noise contaminate seismic measurements made on the earth's surface. It is generally recognized that the noise level is decreased, and improved signal fidelity achieved, if the geophone is downhole. Sometimes a geophone buried only a few inches demonstrates a considerable reduction in noise level relative to one positioned directly on the

earth's surface. This is one of the advantages of vertical seismic profiling, i.e. a geophone can be rigidly locked at great depths in a VSP survey and thus avoid several of the common surface noise problems. However, there are noise problems that are unique to a VSP: related to geophone coupling, cable waves, tube waves, electrical power transmission lines, etc. It is very important to decrease these noise levels for obtaining a quality VSP section.

The VSP data on which I worked were collected in active mining camps. So powerlines and generators were the main noise sources in these data, and they generated strong monofrequency noises (60, 180, 300 Hz). Notch filters applied in time domain (Adam et. al. 1995) were applied to remove this noise (figure 2.1). Following the monofrequency removal, the data were resampled from 0.1 to 0.8 ms and bandpass filtering (60/70-150/180 Hz) were applied. Figure 2.2 shows the three components of the VSP data after noise removal and bandpass filtering.

2.3.3. Downgoing and Upgoing Waves

From the VSP acquisition geometry, VSP waves can be divided into two types: downgoing and upgoing waves. The direct arrivals are called the downgoing waves, while the reflection are upgoing waves as shown by their opposite apparent dip in the display of the VSP data.

The analysis of upgoing wave modes is particularly important since it is these events that are

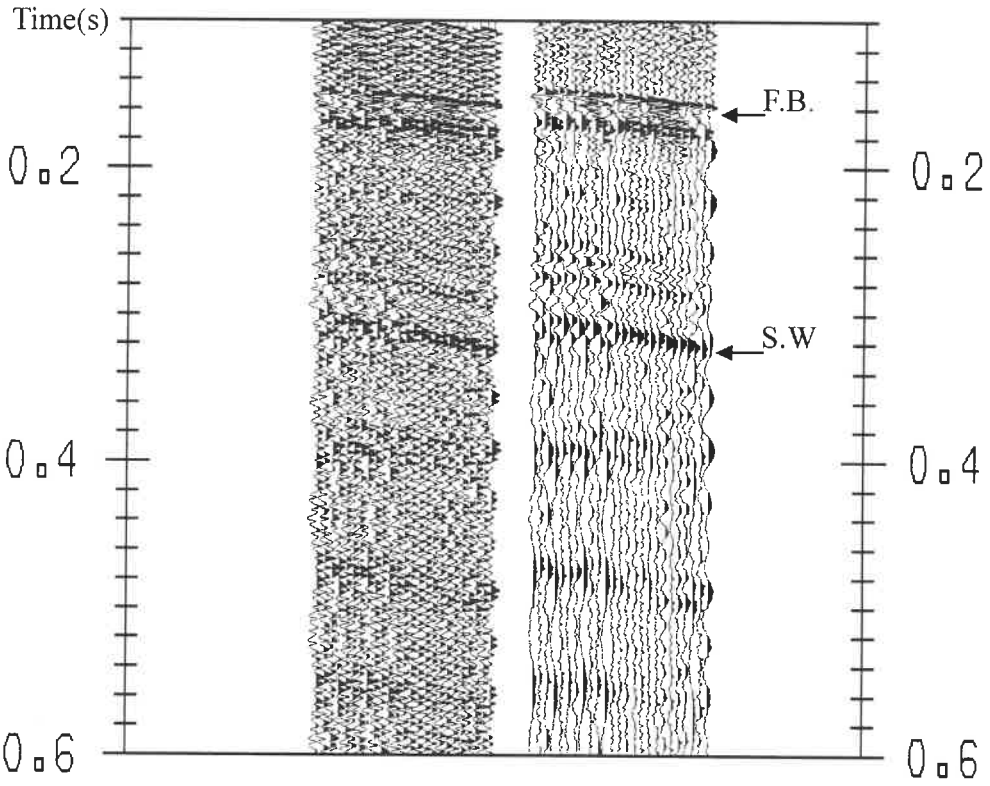

Figure 2.1 Removing 60, 180, 300 Hz noise from the VSP data.
Left: before removal; Right: after removal.

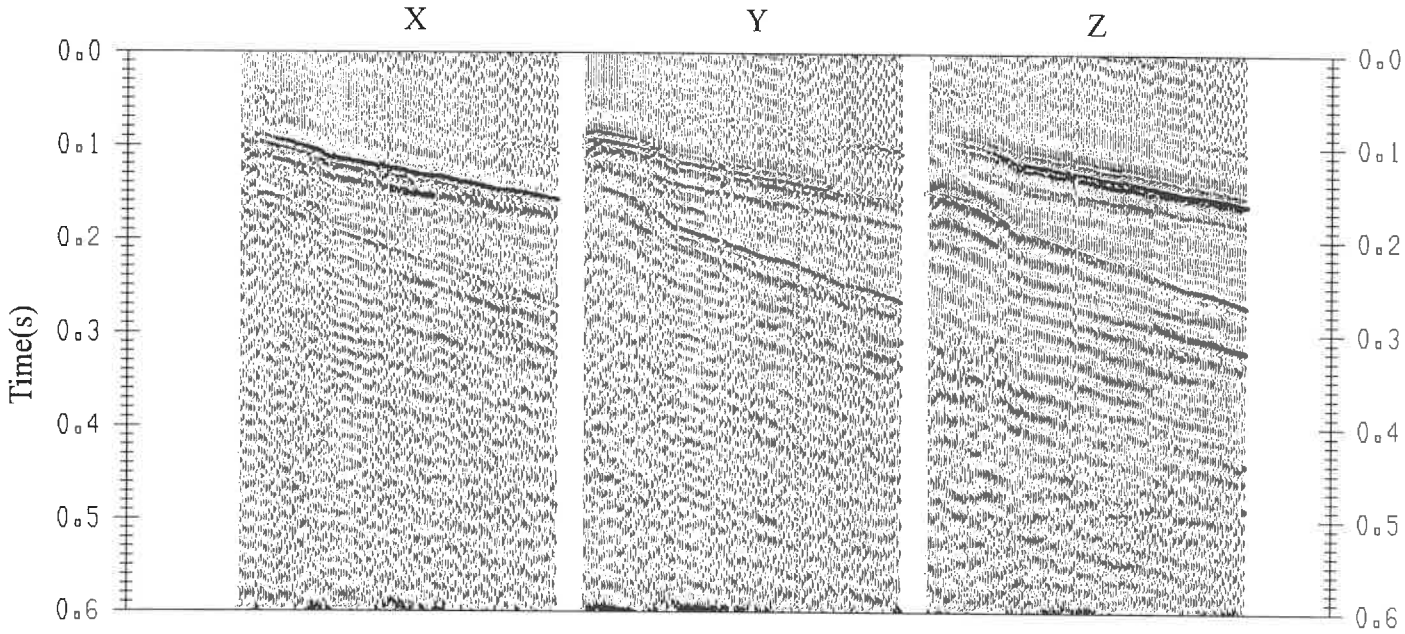

Figure 2.2 The three components of the VSP data

processed to produce the subsurface image. The extraction of these upgoing modes from VSP data is complicated by the fact that they are considerably weaker in amplitude than the downgoing modes. Thus, procedures that can attenuate downgoing modes without seriously affecting upgoing events are essential in VSP data processing. Two approaches were used in this VSP survey: median filtering and f-k velocity filtering.

Median Filter: The term "median" is used here in its correct statistical sense. Median filters perform a type of data smoothing. Let X_1, X_2, X_3, X_4, X_5 represent a sequence of statistical samples having variable magnitudes. Reordering these values so that they successively increase in magnitude will in general create a different sequence, which might for example be X_3, X_4, X_2, X_1, X_5. The median value of this reordered sequence is X_2, the cental value. In this case, the median filter can be represented as:

(X_1, X_2, X_3, X_4, X_5) ---> Median Filter ---> X_2

If the number of the sequence is even, the median filter will usually define the median as the mean of the two middle terms.

The median filtering with subtraction technique for removing the downgoing waves from VSP data can be viewed as following steps: 1) pick up the first arrivals carefully; 2) apply a time shift to the data which is accomplished by shifting each trace by an amount equal to its first break time. The shift horizontally aligns all downgoing modes; 3) a median filter is applied to the data in the horizontal direction along every constant time line. The median filter severely

attenuates all upgoing modes and enhances all downgoing modes; 4) subtract the data from step3 trace by trace from the data produced by step2. This subtraction severely attenuations the downgoing modes in the original data, but does not affect upgoing modes since no significant upgoing modes occur in step2; 5) remove the time shift applied in step1.

A median filter spanning 15 depth levels was applied to the VSP data. Figure 2.3(a) shows the effect of the median filter. The result is not as good as desired. The reason for this is probably that there is no strong upgoing mode in these VSP data.

F-K Velocity Filtering: Sometimes it is necessary after upgoing modes are separated from downgoing, that the upgoing events be further enhanced according to their propagation velocities. A f-k dip filter provides a convenient way of removing other downgoing waves, such as the direct S-wave, without attenuating the upgoing energy. This approach involves the design of velocity filters in frequency-wavenumber (f-k) space. Downgoing energy is arbitrarily defined as having a positive propagation velocity so that the Fourier transform expresses downgoing waves in terms of positive wavenumber. Upgoing VSP energy modes exhibit negative velocities (by arbitrary definition), thus the Fourier transform places all upgoing modes in the negative wavenumber half plane. Hence, the Fourier transform separates VSP events into two different half planes of f-k space, depending on the direction of events travelling, i.e.: upgoing and downgoing VSP modes do not overlap in the frequency-wavenumber domain.

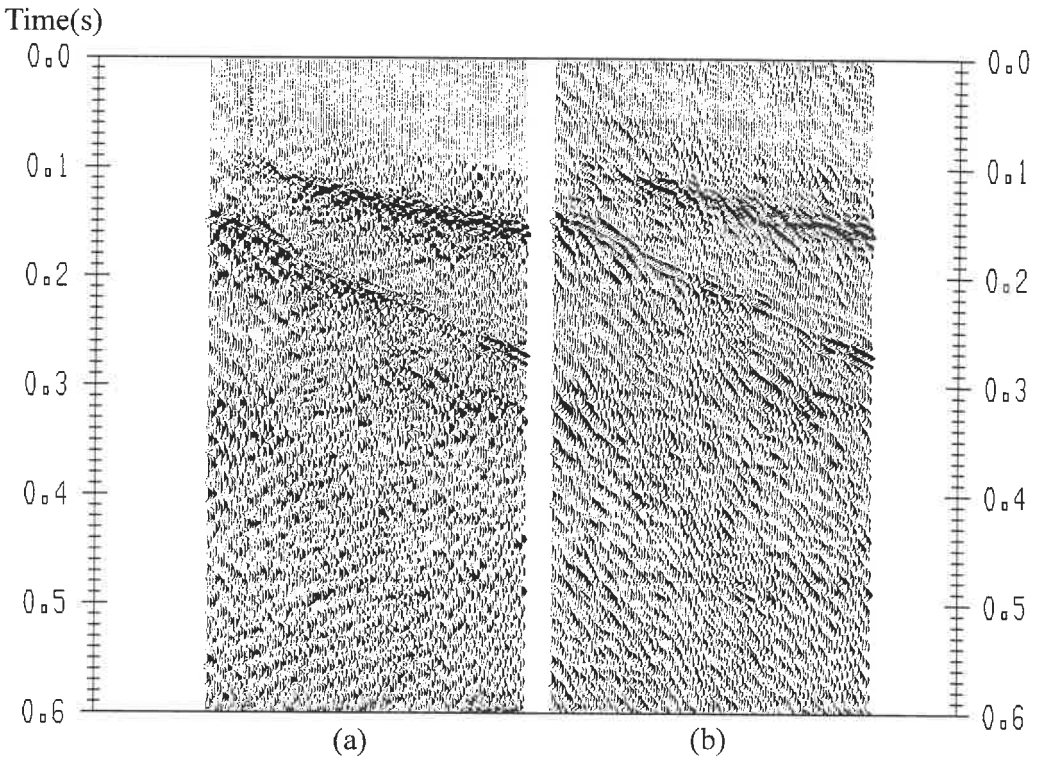

Figure 2.3 Extracting the upgoing wave from the VSP data. (a) after Medi filter; (b) after F-K filter.

Once the data are transformed into the f-k domain, multiplying the data in the positive wavenumber half-plane by a value which is much less than unity will attenuate the amplitudes of the downgoing events. Then performing an inverse Fourier transform on these modified f-k data generates a new VSP data set which is expressed in space and time. The downgoing waves in the new VSP data are much weakened and upgoing waves are enhanced.

Figure 2.3(b), the downgoing waves are attenuated compared to that in Figure 2.3(a). However, the upgoing waves are so weak that they are difficult to see. Thus, the downgoing waves still very strong on the VSP section.

CHAPTER 3

SEISMIC REFLECTION LINE 29-3 AND LINE 93A

3.1 Introduction

The Matagami felsic volcanic complex is part of the Abitibi belt, the largest Archean greenstone terrane on Earth. The Matagami area is host to one of the most productive base metal mining camps in Canada. Many geological studies have been conducted in that area in recent years (Chartrand and Cattalani, 1990). As part of the Lithoprobe project, an 8.72 km and an 8 km high-frequency seismic reflection data were collected along an east-west profile, and a north-south profile, respectively, in the southern part of the mining camp. The data processing for these two lines has been designed to image the geological stratigraphy of that area (Milkereit et al., 1992; Milkereit et al., 1994): the predominantly felsic lavas (rhyolites) of the Watson Lake Group are overlain by the basaltic Wabassee Group. The Key Tuffite is located at the contact between these two groups and dips to the southwest at approximately 45^0. The steeply dipping NS Daniel fault truncates the stratigraphy of the south flank of the mining camp and downfaults the western block. Reprocessing these two high-resolution seismic reflection profiles was carried out in order to obtain a better understanding of this area. Acquisition, reprocessing and interpretation of Line 29-3 and Line 93A are discussed in this chapter.

3.2 Geological Setting

3.2.1. Localization:

The Matagami mining camp is located around 250 km north of Rouyn-Noranda in the Archean Abitibi subprovince. The volcanic stratigraphy of this area is folded into the Galinee anticline which is a NW-SE trending regional fold. On the south flank of the Galinee anticline, the units dip 45^0 to the south-west and are continuous over a strike length of 20 km. On this flank, there are a large number of drill holes which offer excellent geological control. Line 29-3 was shot across the south limb of the Galinee anticline in the west-to-east direction, while Line 93a was in the north-to-south direction (figure 3.1).

3.2.2. Geological Properties & Structures

Many geological surveys have been conducted over the last few decades in this area. A number of positive results have been reported so far (Beaudry et al., 1986; Adam et al., 1992; Milkereit et al., 1992). For the area of Line 29-3 and 93a, from the base to the top, the geological units are divided as: (1) Watson Lake Group (the total thickness is about 2 km), which is composed of a dacitic lava unit with a minimum thickness of 500 m (bottom) and 1500-m-thick quartz porphyritic rhyodacite unit (top) (Piche et al., 1990). (2) Key Tuffite, which consists of chert, some sulfides and very fine-grained felsic tuff. Its thickness is about

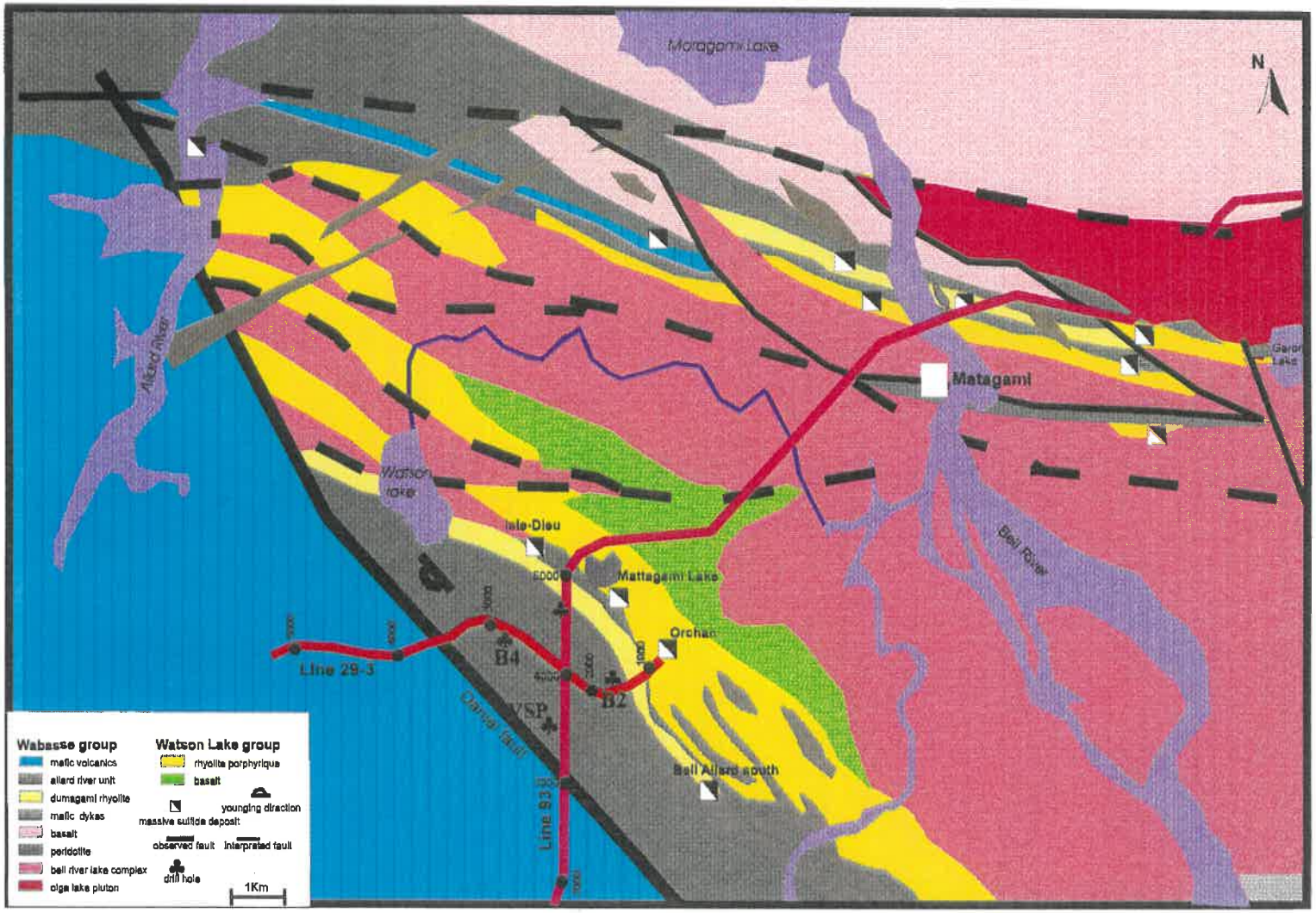

Figure 3.1 Geological map of the Matagami mining camping showing lithological units and the LITHOPROBE seismic reflection profile 29-3 and 93 (modified after Piche et al. 1990).

10 m. It is the level at which most massive sulphide deposits are found in this area. The Key Tuffite is easily recognized by the density greater than 3.0 g/cm^3 because of its sulphide contact. (3) Wabassee Group, which is composed of a lower 500 m unit of mafic and felsic volcanics and an upper unit consisting of andesitic lavas. It is cut by several gabbro sills (Milkereit et al. 1992).

The largest tectonic structure in this area is the Daniel Fault (DF) which trends NW-SE and dips at a moderate angle to the NE. The DF bounds the southern flank of the mining camp. It has a dip-slip displacement of 1 to 2 km (Milkereit et al., 1992).

Since the Key Tuffite and the rhyolite (top of the Watson Lake Group) have similar P-wave velocities the contact between rhyolite and Key Tuffite (Watson Lake Group/Key Tuffite) is not likely to generate a reflection. However, the gabbro in the Wabassee Group and Key Tuffite have large differences in velocity, therefore, the contact between them will generate strong reflections (Gabbro and Key Tuffite have average velocities of 6.5 km/s and 6.0 km/s, respectively). (Adam et al., 1992).

3.3 Data Acquisition

Line 29-3 survey was shot in October, 1990 as part of the Abitibi-Grenville LITHOPROBE project. The line is oriented approximately east-west and extends over a distance of 8.72 km.

The data were collected using vibroseis sources and a multichannel telemetry acquisition system which included in-field stacking, noise-rejection, and correlation capabilities. The vibrator sources used two MERTZ model 18 vehicles with 40,000 lbs peak force. The spacing of the vibration points (VP) was 20 m, a 20-m-long weighted source array used at each VP. Four 12 s linear sweeps from 30 to 140 Hz were recorded at every vibration point.

The receivers (geophones) used were 14 Hz MARK L25 with damping factor 70%. Each geophone group comprised 9 geophones spaced 2.5 m apart. The total receiver spread employed 240 receiver groups spaced every 20 m resulting in a nominal fold of 120. A split-spread geometry was used, with a near offset of 0 and far offset of 2400 m. There was no gap between source and receivers.

The recording instrumentation was a 240 channel SERCEL SN368 system. The lowcut filter is 0 and the highcut filter is 178 Hz. No notch filters were applied. For each "shot", 4 successive sweeps were recorded such that 60 Hz powerline noise was attenuated in the vertical sum of all four sweeps and other noise was also suppressed. The data were recorded to 4 s at a sample interval of 2 ms (table 3.1).

Data Acquistion for Line 93a is very similar to Line 29-3. The basic parameters of its data acquisition are presented in table 3.2.

Table 3.1: Data Acquisition Parameters for Line 29-3:

SOURCE:	
Source Type	Vibroseis, MERTZ 18B
Peak Force	40,000 lbs
Source Pattern	2 Vibrators over 20 m
Source Interval	20 m
Source Sweep	12 s
Repetition	4
Source Frequencies	30-140 Hz linear
RECEIVERS:	
Geophones Type	MARK L25
Damping	70%
Geophone Interval	20 m
Geophone Layout	9 over 2.5 m
Spread	119R-R/S-120R or 120R-R/S-119R, no gap
No. of Traces	240
Min. Offset	0
Max. Offset	1400 m
ACQUISITION SYSTEM:	
Instrument	240 Channel SERCEL SN368
Field Filter	178 Hz High-cut
Record Length	4 s
Sample Rate	2 ms

Table 3.2: Data Acquisition Parameters for Line93a:

SOURCE	
Type	Vibroseis
Array	Two vibes over 12 m, moving up 8 m
Interval	20 meters
Spread Array	120R VP 119R
Sweep	30-140 Hz; 4 sweeps×12 seconds
INSTRUMENTS	
Type	MDS-18X
Number of channels	240
Record Length	16 sec
Sample	2 ms
LowCut Filter	out
HighCut Filter	out
Notch	out
RECEIVER	
Geophone Type	Mark L25
Frequency	30 Hz
Spacing	9 over 8 m
Group Interval	20 m

The Rayleigh resolution limit is one-quarter of the domain wavelength (e.g. Sheriff, 1982). This means that although a layer with a thickness of less than one-quarter wavelength can still produce reflections, its thickness cannot be reliably determined from the wave shape. Since the data were recorded at frequencies between 30 Hz and 140 Hz, and taking the centre frequency of the sweep, 85 Hz, to be the domain frequency, and the average velocity of basement rocks to be 6000 m/s, the vertical resolution is about 18 m.

3.4 Data Processing

The ITA INSIGHT software package was used for all of the data processing, and a traditional reflection data processing sequence was applied. The most challenging processing for both lines was the correction for varied overburden conditions (refraction statics corrections) and the imaging of steeply dipping structure (DMO and CROSSDIP corrections for Line 29-3. DMO corrections for Line 93a).

3.4.1 Crooked Line Geometry

Before applying any data processing to a seismic line, a correct geometry of the line must be setup and checked. To do this in INSIGHT, two formatted files are used: one containing survey information and the other containing the observer notes. The two files are interactively created and edited with two different programs (Build_obs and Build_sur). The program MOD_HEADER transfers this information from the geometry files into the trace headers and sets CDP locations assuming a straight line.

For a crooked line (such as Line 29-3), the module CDPBIN is used to design a so-called slalom line along which the centers of the CDP bins are located. Different CDPBIN widths and heights yield different CDP fold. A "glue distance" moves slalom points onto stations if they are close to a station. For Line 29-3, three slaloms lines which are in different directions

are designed. The CDPBIN widths are chosen to cover almost all of the CDPs so that approximately 100 CDP fold is obtained (figure 3.2).

The CDPTOSS program is used to fix the "mistakes" made by MOD-HEADER in assigning CDPs for the crooked line, and flags the unbinned traces as dead.

3.4.2 Noise Analysis

A noise analysis map for Line 29-3 was calculated to identify noise traces, bad shots or bad stations, and especially to check geometry errors within the survey file.

The noise analysis is based on an amplitude analysis performed on a trace by trace basis, using a Fourier decomposition within a running time windows (Senechal et al., 1995). Considering a time window of N points centred at time t_j, its average amplitude in the time domain is given by:

$$s(t_j) = \frac{1}{N+1} \sum_{t=t_j-\frac{N}{2}}^{t_j+\frac{N}{2}} |s(t)| \qquad (3.1)$$

Assume that the amplitude level at later time is representative of the random noise level during the acquisition because the relative amplitude at later time are comparable to those observed at beginning of the records, before the first arrivals. I have estimated the noise level

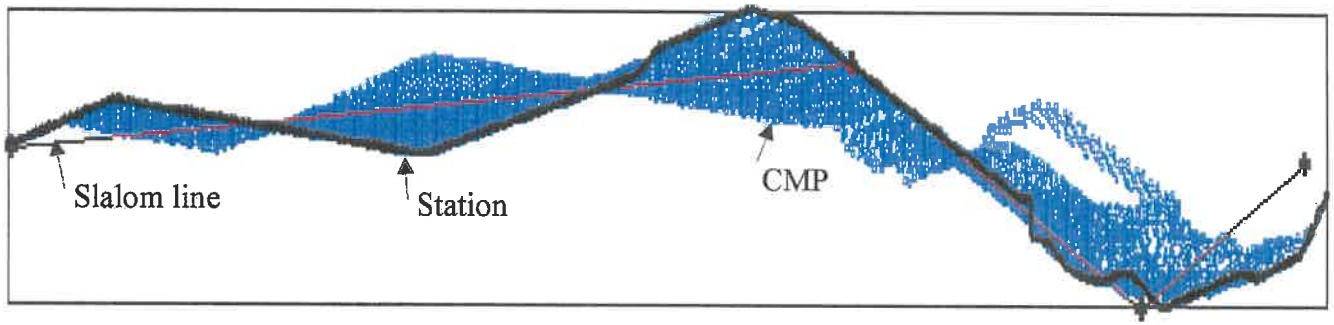

Figure 3.2 The crooked line 29-3.

for each shot-receiver pair using the equation (3.1) with a window from 1.7 s to 2.0 s and plotted the results on a stacking chart with MATLAB software (figure 3.3). Warm colours correspond to higher noise levels. If there is an offset in the noise pattern at a certain station, there is probably an error in the survey file.

In figure 3.3 the warm coloured line in the middle of the chart represents the shot points. Low shot point and low station numbers correspond to the east of the line, while high shot point and high station numbers correspond to the west. Analyzing this chart, three observations can be made: (1) In the east, there is a shot point shift between stations 106 and 126. This corresponds to the first shot gap (20 shots are missing, probably because of houses, buildings in this area, which restrict "shooting"). The second shot gap is relatively small and it is between stations 283 and 287 (4 shots missing). (2) The whole section appears largely noise free, although some small groups of traces are noisy. This is probably due to power lines and generators (120 Hz, 60 Hz, 45 Hz noise) (figure 3.3(a)). After removing this electrical noise by notching, the map looks clearer (figure 3.3(b)). However, there still exists one (the only one) "big" noise area located between stations 180 and 230. This noise is related to intense mining activity. (3) There is no noise shift with a certain station. Therefore, the geometry survey file is correct.

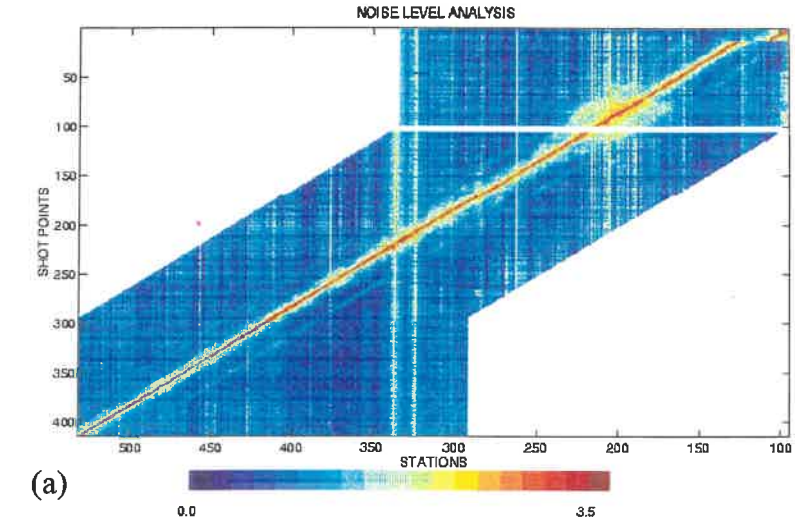

(a)

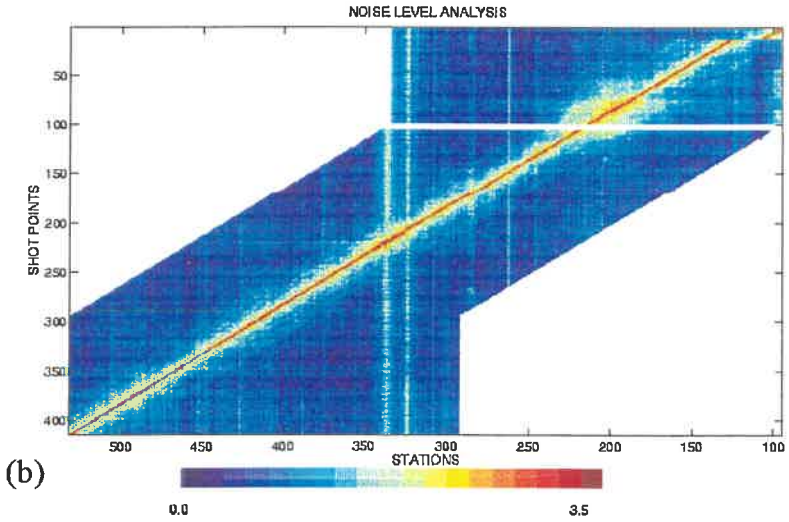

(b)

Figure 3.3 Noise analysis on Line 29-3. (a) before noise removal; (b) after noise removal.

3.4.3 First Arrivals & Shear Wave

The first break picking is an important step because the quality of refraction statics depends greatly on its precision. Since Line 29-3 data was shot in an active mining camps, powerlines, generators, pumps etc. generate very strong monofrequency (60 Hz, 120 Hz, 45 Hz) noise (some exceeding 40 dB) so that the first breaks are obscured (figure 3.4(a)). Picking of some shots is impossible. Therefore, it is necessary to remove these noises before picking. Notch filters applied in time domain (Adam, 1995) were applied for this purpose. Figure 3.4(b) shows that the filtered gathers reveal clearer first breaks. Following the noise removal, carefully picking and double checking were done, providing confidence in the accuracy of the first breaks.

The first breaks in a shot gather are composed of a direct wave (for near offset) and refracted wave (for far offset). Figure 3.5(a) is a typical shot gather of Line 29-3. The first breaks comprise a direct wave(< ~100 m) implying a velocity for weathering layer of about 900 m/s (from the slope of the direct wave). The first arrivals for greater offsets (> ~100 m) are a refracted wave, giving a bedrock velocity of around 6000 m/s (from the slope of the refracted wave).

The amplitudes of the first breaks and S-wave are very high compared to that of underlying reflected arrivals, which may be abscured. For this reason, removal of the first breaks (usually

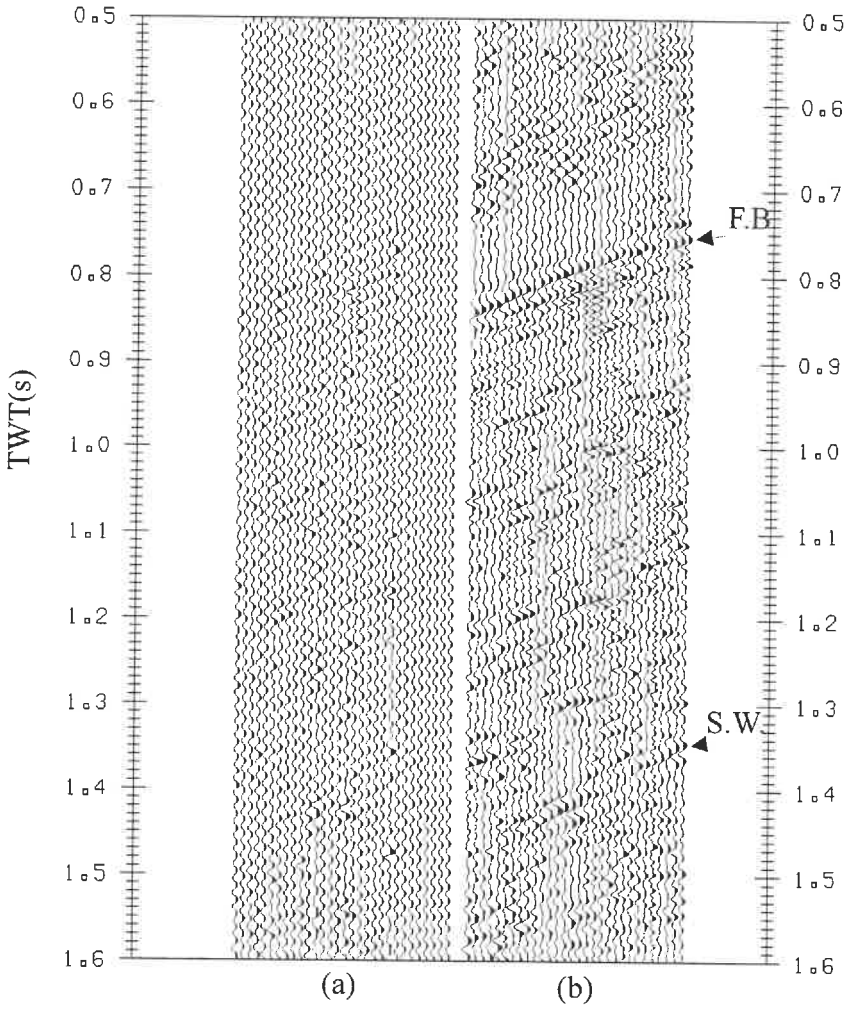

Figure 3.4 Removing 45, 60, 120 Hz noise. (a) before removal; (b) after removal.

called first break mute) and the shear wave is important in order to recover reflections at shallow times.

The main method for the above purpose in the processing of Line 29-3 data processing is a median filter. The median filter scans a pre-specified number (9, 13, 15 etc.) of traces and replaces the amplitude at the middle trace with the median of the scan window. The algorithm slides the scan window across all traces in the record at each time sample to produce the filtered record. If we assume that events of interest are horizontal, the median filter will smooth structures across a section (Hardage, 1985).

To remove the first breaks, firstly, I aligned the first breaks according to the picks; secondly, I flattened the data to 0.3 s and removed any residual misalignment by trim statics; thirdly, I applied a top mute before 0.25 ms and bottom mute after 0.35 ms, following a median filter (15 traces in size); finally, I subtracted the median filtered data from the data only having the first and the second steps, then removed the trim statics and unflattened the data back to "normal" shot gather.

To remove the shear wave, the steps involved are: (1) estimating the shear wave arrival times for each trace by dividing the offset by the shear wave velocity ($t = \Delta x / v$, $1/v = 0.00028$); (2) flattening the data to 0.3 ms and applying a trim statics; (3) applying the median filter (15 traces in size); (4) subtracting the median filtered data from the data before median filter; (5)

removing the trim statics and unflattening the data back to "normal". Figure 3.5 compares before and after first break muting and S-wave removal for a particular shot (shot 205).

In addition, NMO-stretch muting is combined to remove the first breaks. Normal moveout stretches the time axis of the far offsets more than that of the near offsets in order to align a reflection with the zero-offset reflection time; the greater the stretch, the lower the frequency of the signal. The INSIGHT NMO program provides an option to mute data stretched more than a certain percentage during stacking. Several values (0.5, 0.6, 0.7, 0.8, 0.9) have been tested. The best result is achieved by muting stretching of greater than 60%.

3.4.4 Refraction Statics

Reflection times are often affected by irregularities (both elevation and velocity) in the near surface. This effect will distort the regular hyperbolic moveout so that the stacking quality is degraded. It is necessary to correct for such effects. Usually, refraction-based statics corrections (including reference datum and weathering corrections) remove long and short wavelength anomalies, and reflection-based residual statics corrections remove any remaining short wavelength static shifts.

Many methods exist for refraction statics. The most popular one is the so called ABC method (Hagedoorn, 1959). It involves picking the first break, deriving the intercept time and bedrock

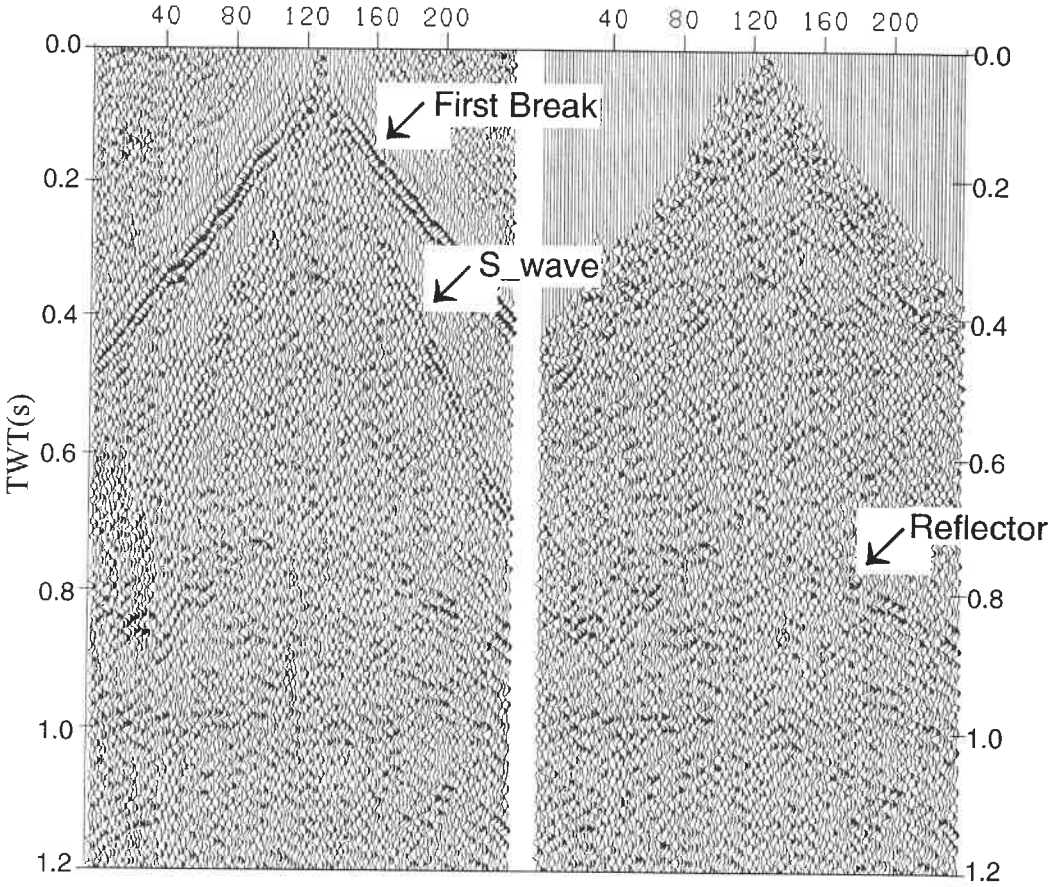

Figure 3.5 A typical shot (205th) of Line 29-3 before and after first-break and shear-wave removal. Left: before removal; Right: after removal.

velocity, assuming a weathering velocity, and computing the static shift for each station (shot or receiver). But this method usually has problems when more than one weathering layer is present. Hampson and Russell (1984) developed an new method which solved this problem by applying generalized linear inversion (GLI). The GLI method iteratively modifies the model parameters (such as velocities and thicknesses) to minimize the difference between the computed and observed travel times so that good refraction statics are obtained.

In our laboratory, four softwares (REFSTAT, REFSTAT1, REFSTAT2 (in INSIGHT), GLI3D (not in INSIGHT)) are available for refraction statics. The first three are based on the ABC algorithm. As mentioned above, because they have multiple weathering layers problem, three of them got poor refraction statics results on Line 29-3. However, GLI3D, which is based on generalized linear inversion theory, gave excellent refraction statics corrections for Line 29-3. The datum elevation of 300 m, a weathering velocity 900 m/s, and a replacement velocity of 6000 m/s were used. By adjusting the velocities and the thicknesses, the average actual first-break picks (observed travel times) and the computed travel times are almost aligned along the same line (figure 3.6), implying the difference between the computed and observed travel times are small. The average difference between them is 3.28 ms. Figure 3.7 shows the final model for the refraction statics of Line 29-3. The total refraction static corrections of Line 29-3 (including datum corrections) for receivers and shots range from -98.0 to -2.0 ms (figure 3.8). To check this correction, I examine the first breaks throughout the whole line. A comparison of the stacked sections with and without refraction static

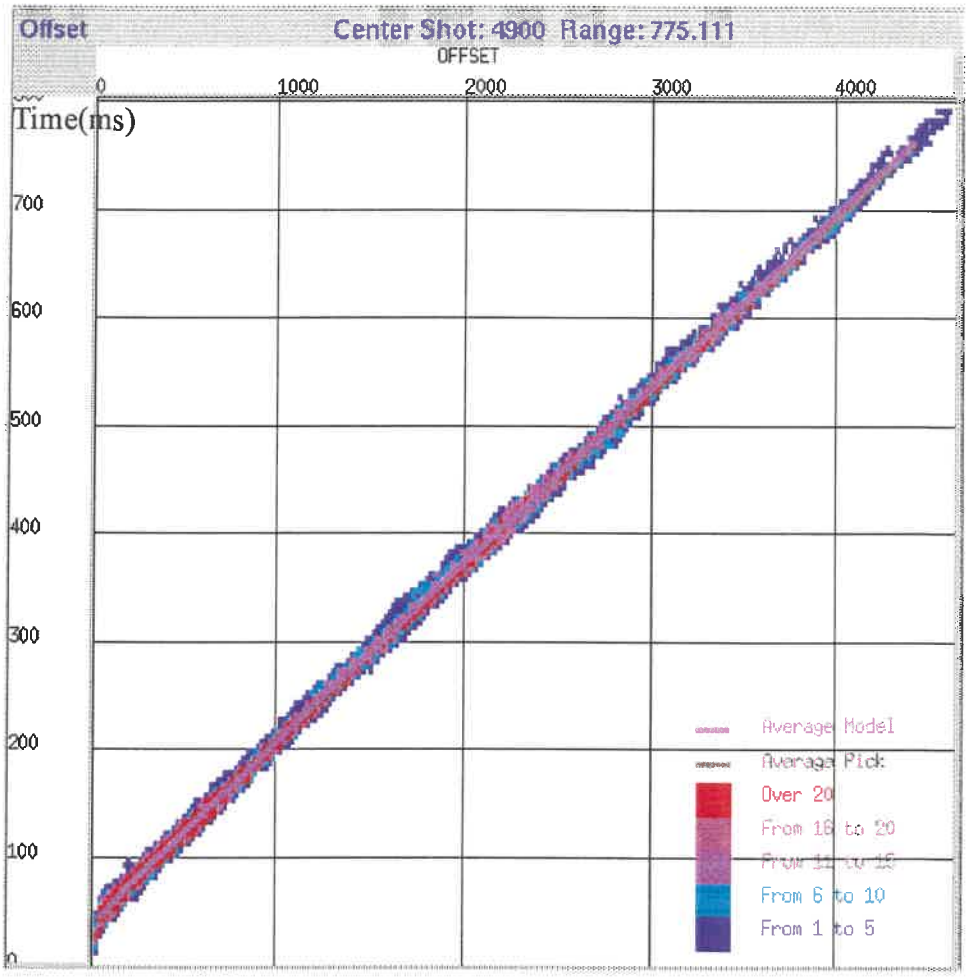

Figure 3.6 The computed and observed first-break travel times of Line 29-3.

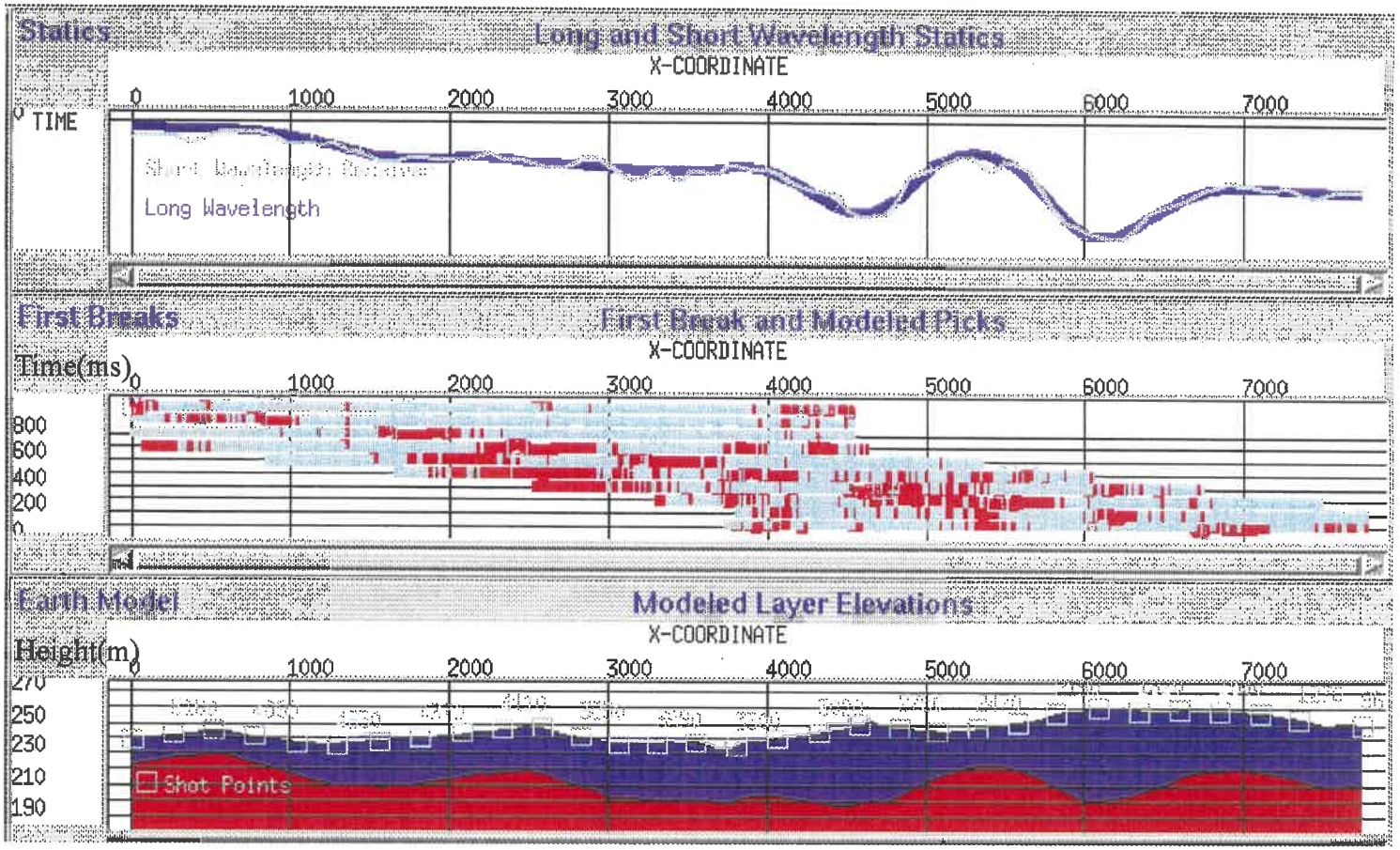

Figure 3.7 The refraction statics model for Line 29-3.

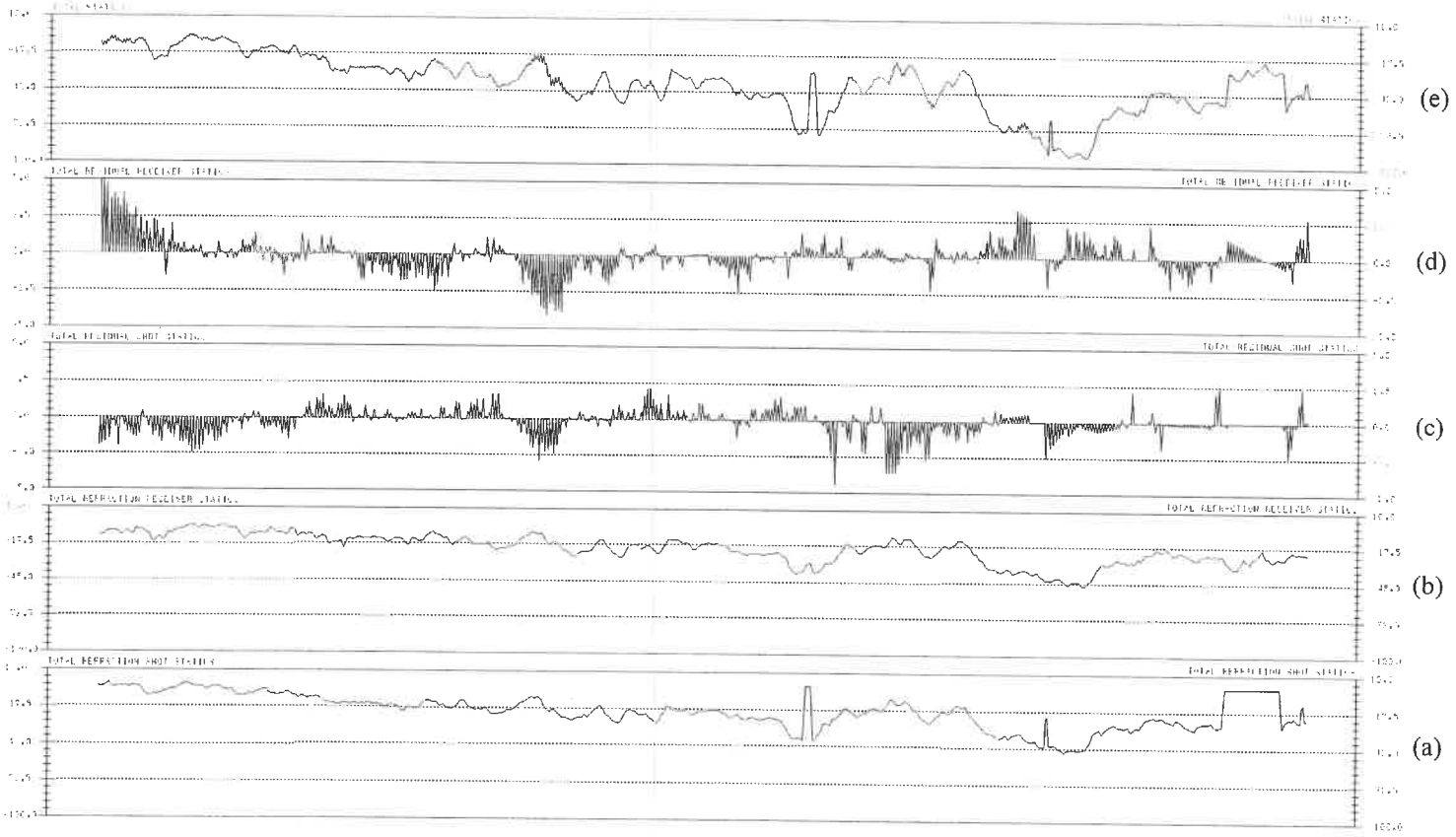

Figure 3.8 The statics corrections for Line 29-3. (a) total refraction shot statics; (b) total refraction receiver statics; (c) total residual shot statics; (d) total residual receiver statics; (e) total statics.

correction is shown in figure 3.9. As expected, the first breaks are aligned by refraction statics. Between 1800 CDP and 3000 CDP, there are small variations on short wavelength. That is because the first breaks are hardly picked correctly in this range. These variations will be fixed by residual statics. Figure 3.10(a) is the brute stack, and (b) is the stack after refraction statics corrections for 950-3200 CDP between 0.0 s and 0.8 s. A significant improvement on the stack section was achieved, in terms of reflection continuity and reflection amplitude between 0.2 s and 0.5 s. Figure 3.11 is another part of Line 29-3 showing the changes before and after the refraction static corrections. The reflectors at 0.35 s under CDPs 4500-4200 and 3600 were recovered after the corrections; The structure crossing this whole portion between 0.45 s and 0.8 s appears stronger after the corrections; Finally a few reflections between 0.6 s and 1.2 s are recovered and enhanced after the corrections.

The refraction statics for Line 93a is also done by the GLI3d. The same procedure was applied with Line 29-3. The statics of this line are up to -70 ms (including datum corrections). Figure 3.12 is the model for its refraction statics. The statics effect is shown in figure 3.13.

3.4.5 Cross-dip Analysis

Conventional common-depth-point (CDP) processing requires the assumption that receiver groups and shotpoints are distrubuted along a straight survey line. In practice, however,

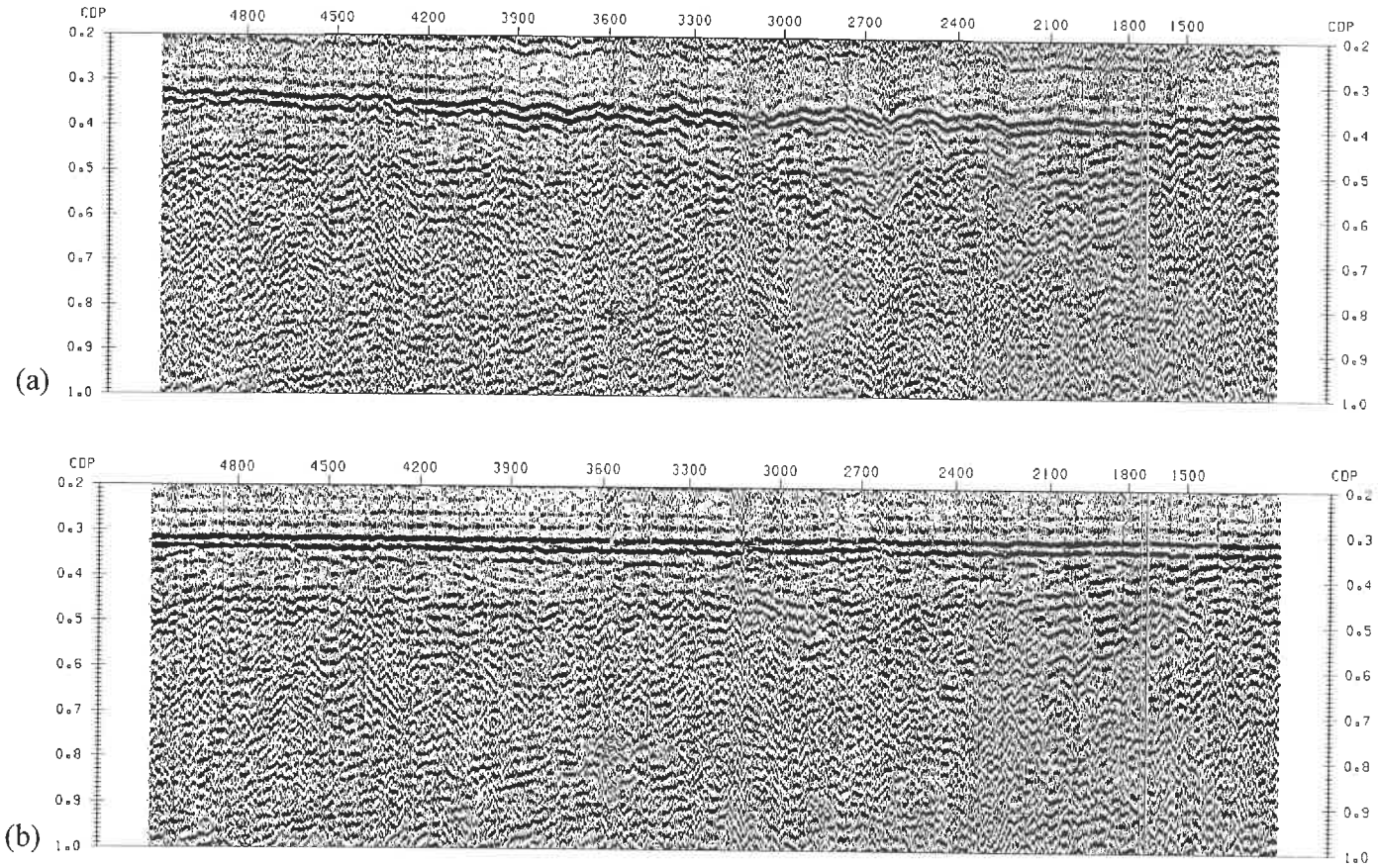

Figure 3.9 The effect of refraction statics on Line 29-3. (a) before statics; (b) after statics.

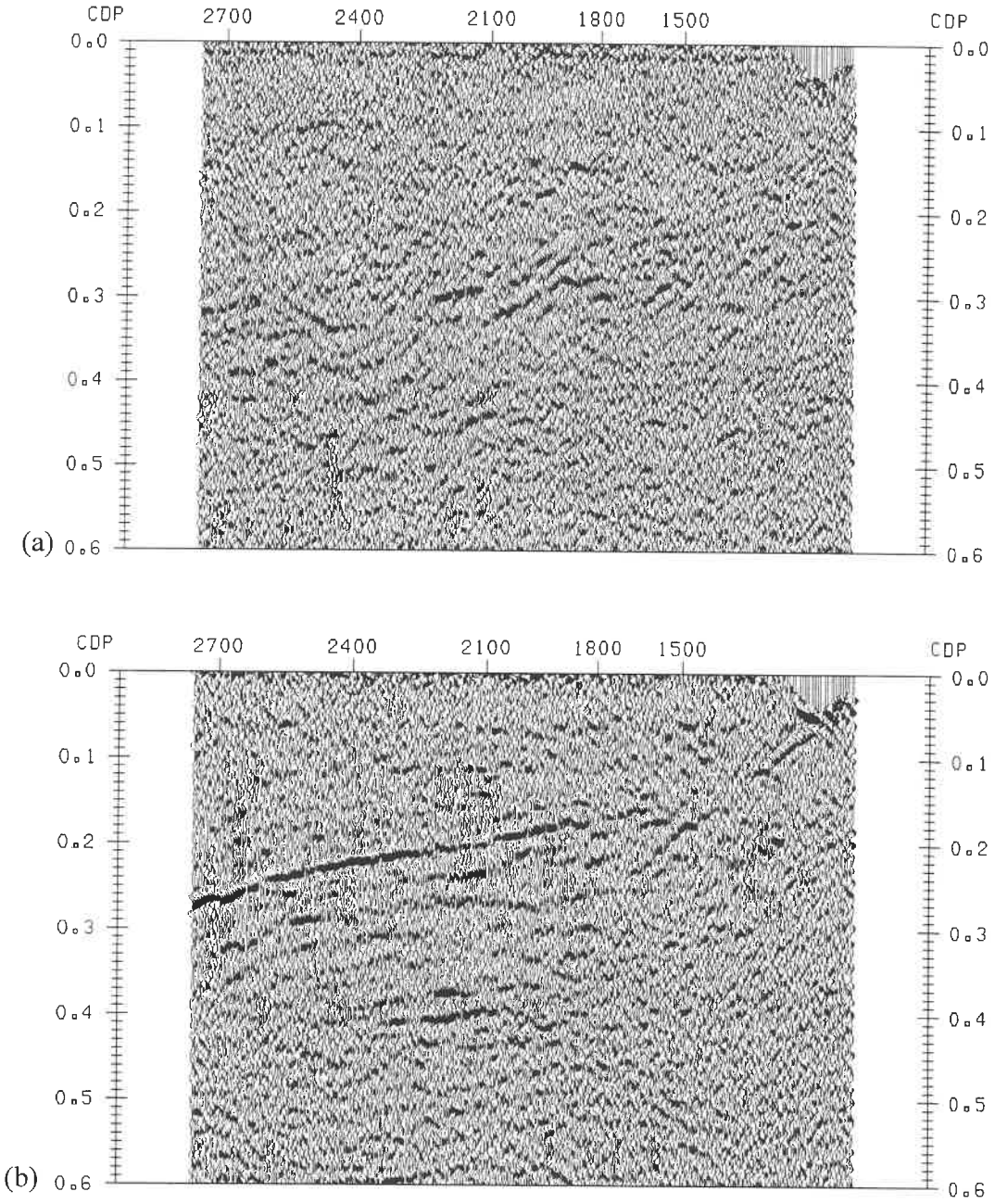

Figure 3.10 The effect of refraction statics on the 950-2800 CDP of Line 29-3. Above: before statics; Below: after statics.

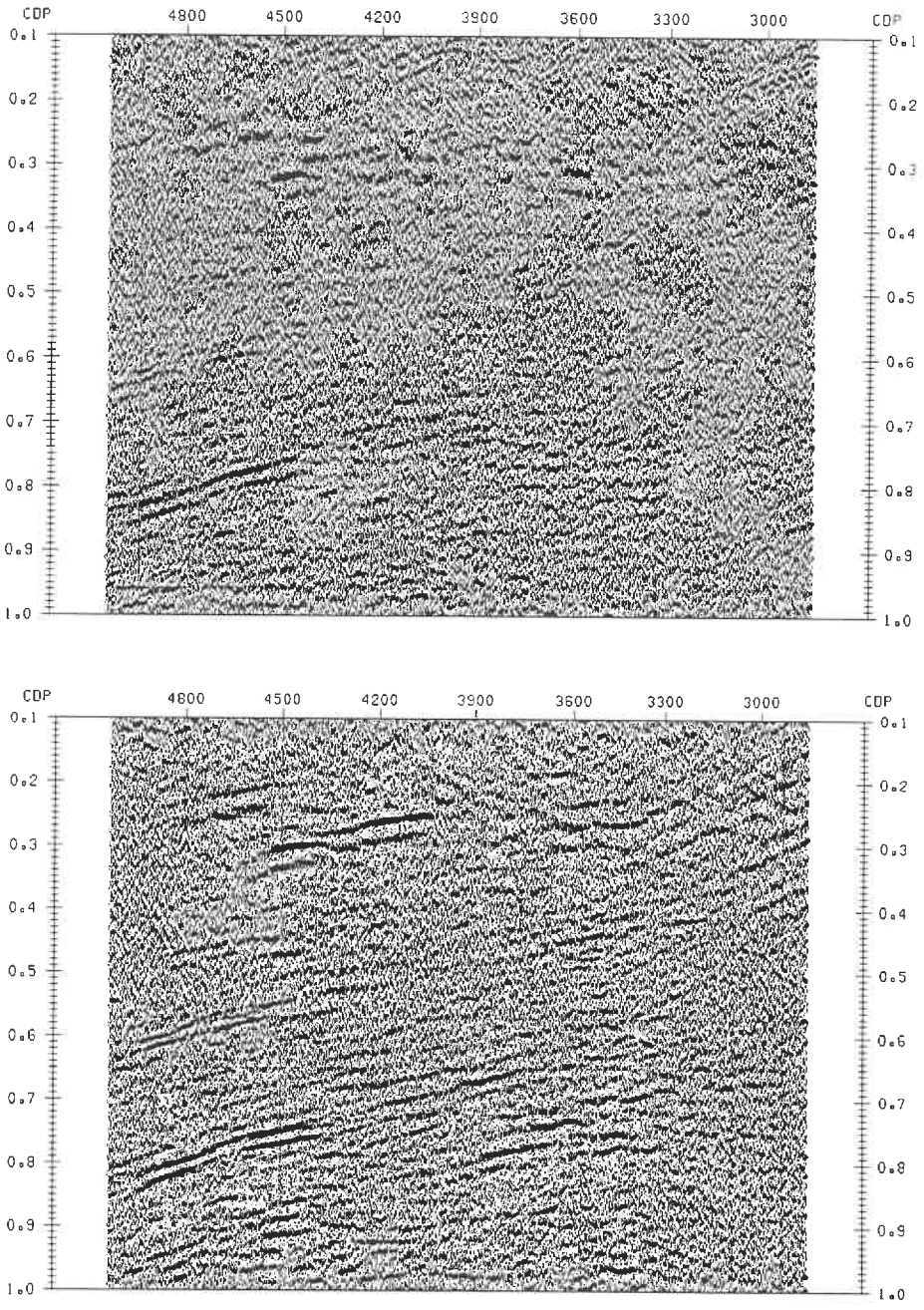

Figure 3.11 The refraction statics on the 2900-5100 CDPs of Line 29-3
Above: before statics; Below: after statics.

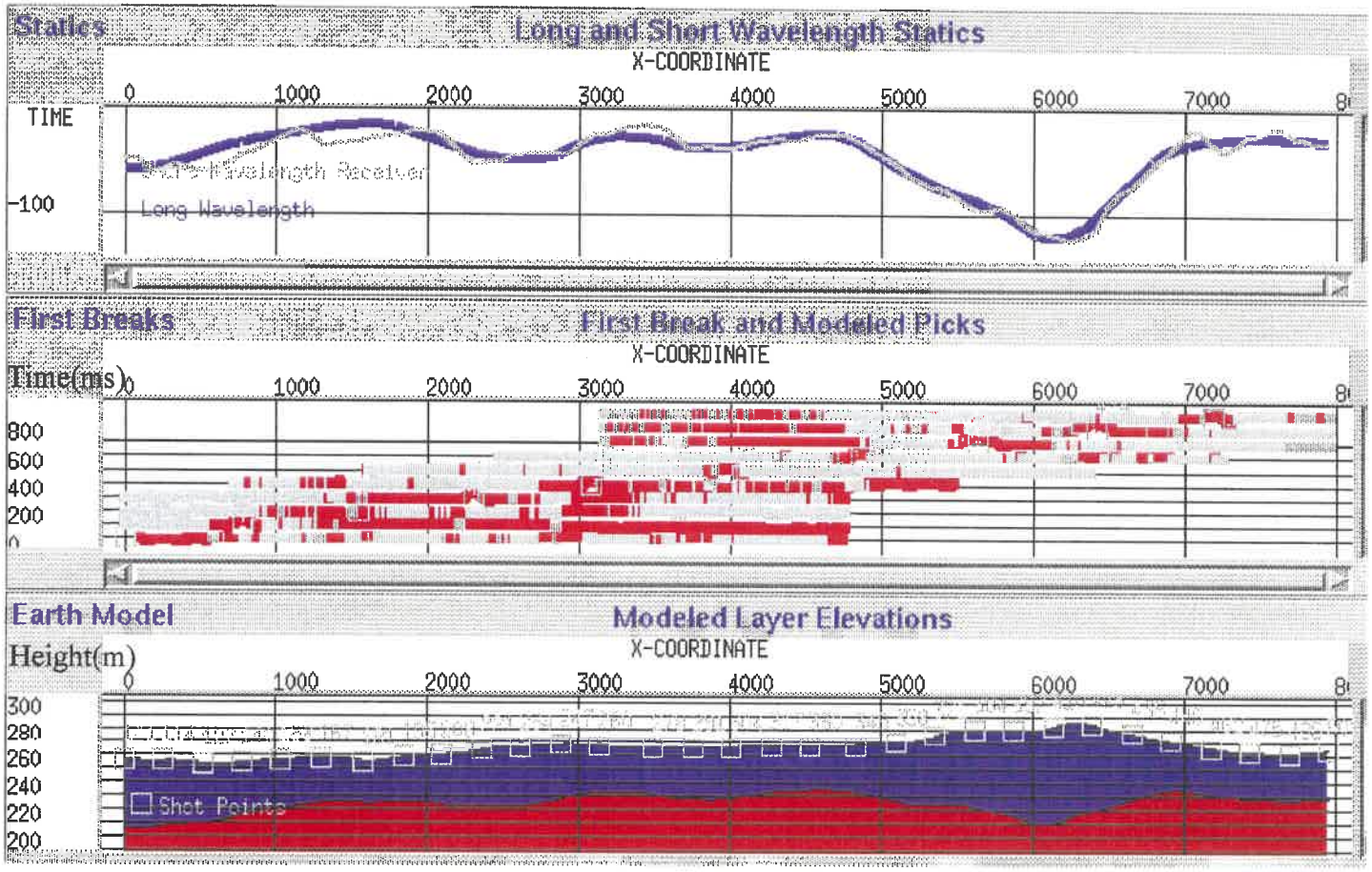

Figure 3.12 The refraction statics model for Line 93a.

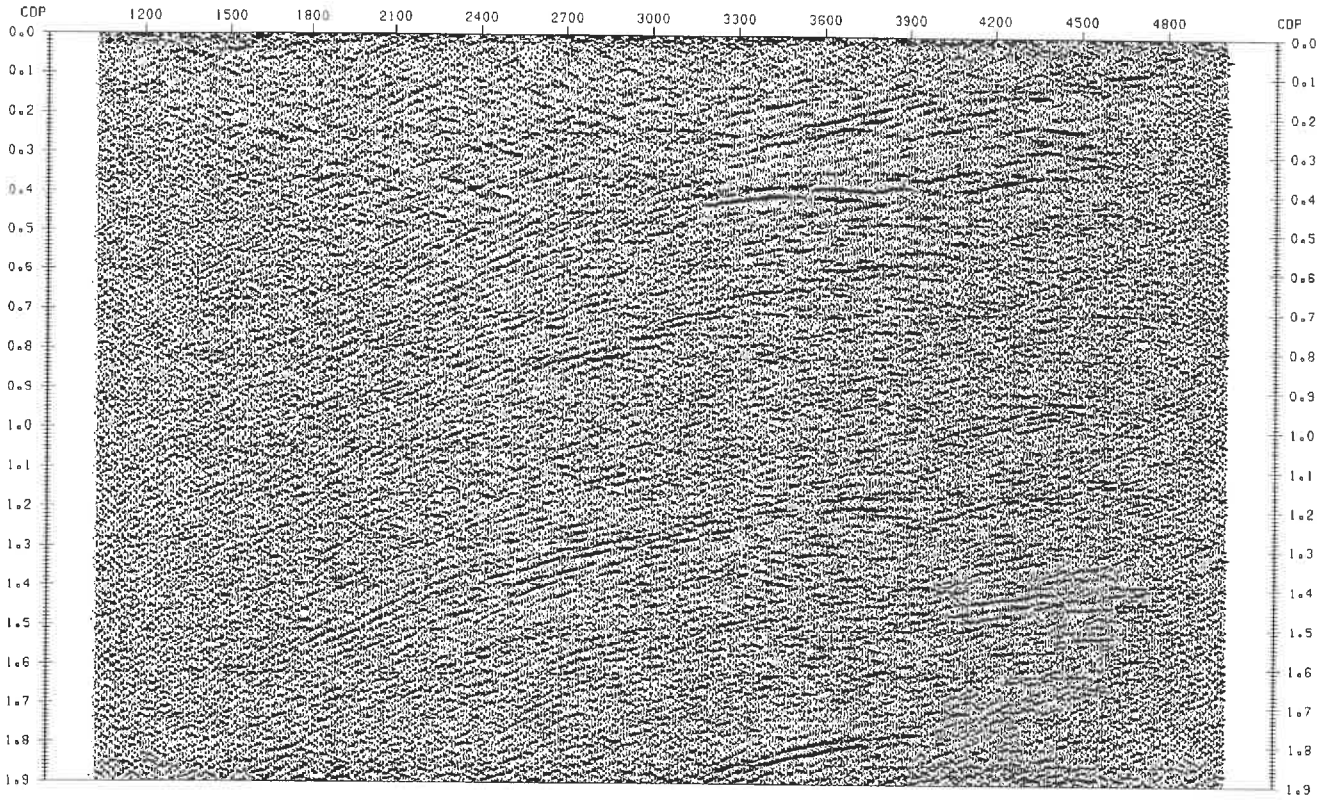

Figure 3.13 The stacked section of Line 93a after refraction statics.

existing road networks or surface topography often result in a crooked acquisition line.

When survey lines are crooked, the midpoints between shotpoints and receiver locations are scattered in both in-line and cross-line directions. These scattered midpoints invalidate the concept of a common midpoint gather of traces. To solve this problem, we usually create a new line for processing, which typically is a smooth curve that follows the local mean of the midpoint positions or a number of straight line segments. Then we sort the seismic traces into new gathers that relate naturally to points along the new processing line. After sorting to CDPs along the processing line, the midpoint scatter is entirely perpendicular to the local direction of the effective line (Larner et al. 1979).

If the effective line is strictly a dip line, the midpoint scattering doesn't affect the quality of the CDP stack. If, however, the subsurface interfaces have components of crossdip (crossdip is the component of dip normal to the local profile direction), variations in reflection times compared to a straight survey line occur. Traces within a CDP gather whose midpoints are relatively downdip will show longer reflection times than traces with midpoints updip. Therefore, we must apply crossdip corrections to the data to improve the stacking quality. The equation for crossdip correction is:

$$\delta t_{ij} = \frac{2Sin\gamma_k}{v_k} Y_{ij} = D_k Y_{ij} \qquad (3.2)$$

where $D_k = 2 \text{ Sin } \gamma_k / v_k$ is constant for a given CDP k; γ_k is crossdip angle at CDP k; V_k is velocity at CDP k; i is shot number under consideration; j is receiver number under consideration.

Line 29-3 is crooked. The processing line was chosen to be three line segments to make easier crossdip analysis. For each of these lines, I calculated the crossdip distance of traces (Y_{ij}) in a CDP from the slalom line and put the value in header word 19. Time corrections according to equation (3.2) were applied. First, I estimated the crossdip angle γ_k to get D_k roughly. Then in a certain range, a variety of values were tested to find the crossdip correction that worked best for each of subsurfaces. Table 3.3 gives the best crossdip correction parameters (D_k) for Line 29-3. As expected, the stack quality of Line 29-3 is quite improved by the crossdip corrections for many reflectors (figure 3.14). Especially, the east dipping event between 0.75 s and 1.25 s under 4500-1800 CDPs is more continuing and strengthened after crossdip correction.

Since Line 93a is a straight survey, the midpoints between shots and receivers are not scattered. So crossdip correction for Line 93a is unnecessary.

Table 3.3: The Crossdip Corrections for Line 29-3:

CDP	Two-way Time(s)	D_k Value
2675	0.0 0.5 1.2	-2.0E-5 -2.0E-5 -8.0E-5
3225	0.0 0.5 1.2	-4.0E-5 -4.0E-5 -8.0E-5
4010	0.0 0.5 1.2	-10.0E-5 -10.0E-5 -8.0E-5
4780	0.0 0.5 1.2	-8.0E-5 -8.0E-5 -8.0E-5

3.4.6 Residual Statics

The goal of seismic reflection data processing is to obtain a quality stacked section. Statics are a key step. Application of incorrect static shifts will decrease the power of the CDP stack. Although refraction statics can remove most of the time anomalies caused by near surface lateral velocity variations, topographical changes, and low velocities in the weathering layer, residual statics are still necessary in most cases because of errors arising from assumptions in the models that underlie refraction statics methods, and mispicking of first break times.

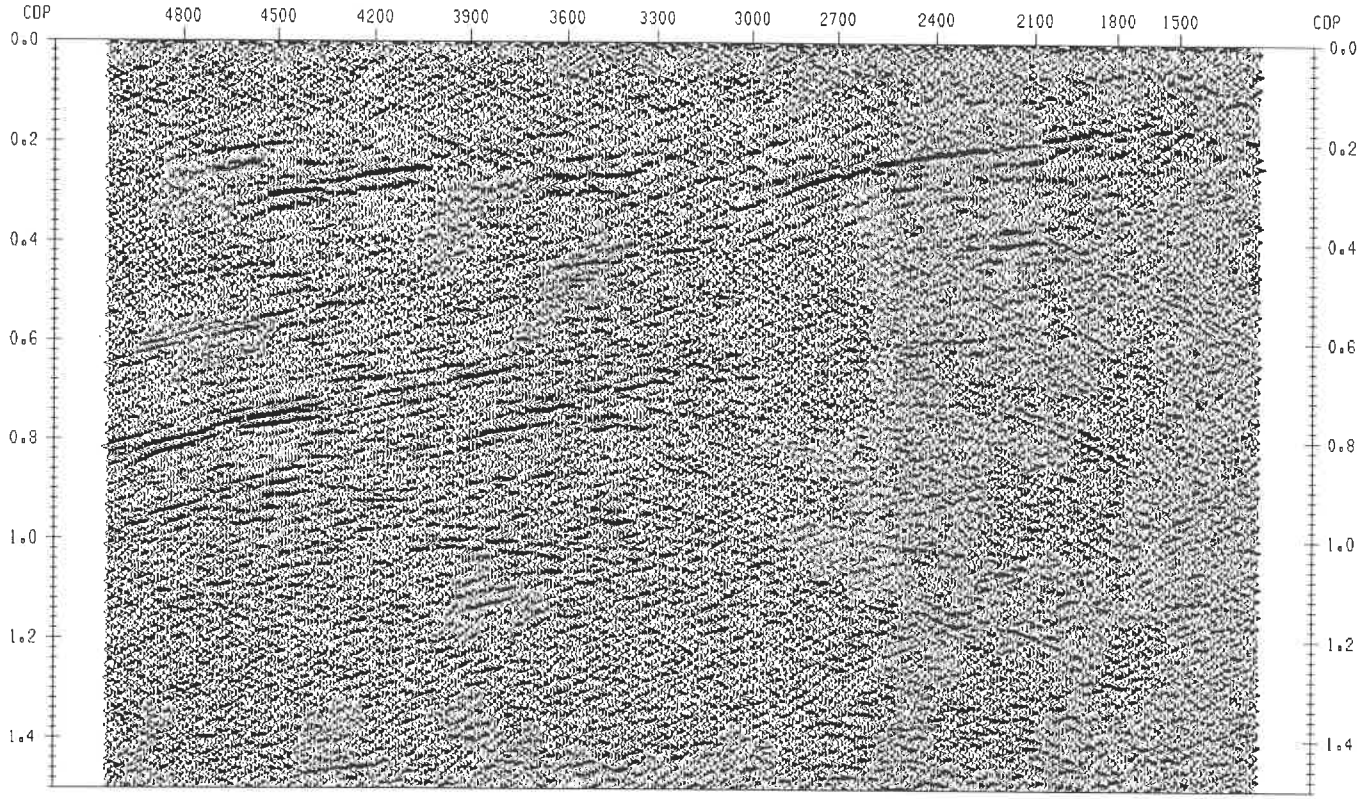

Figure 3.14a Line 29-3 before the crossdip corrections.

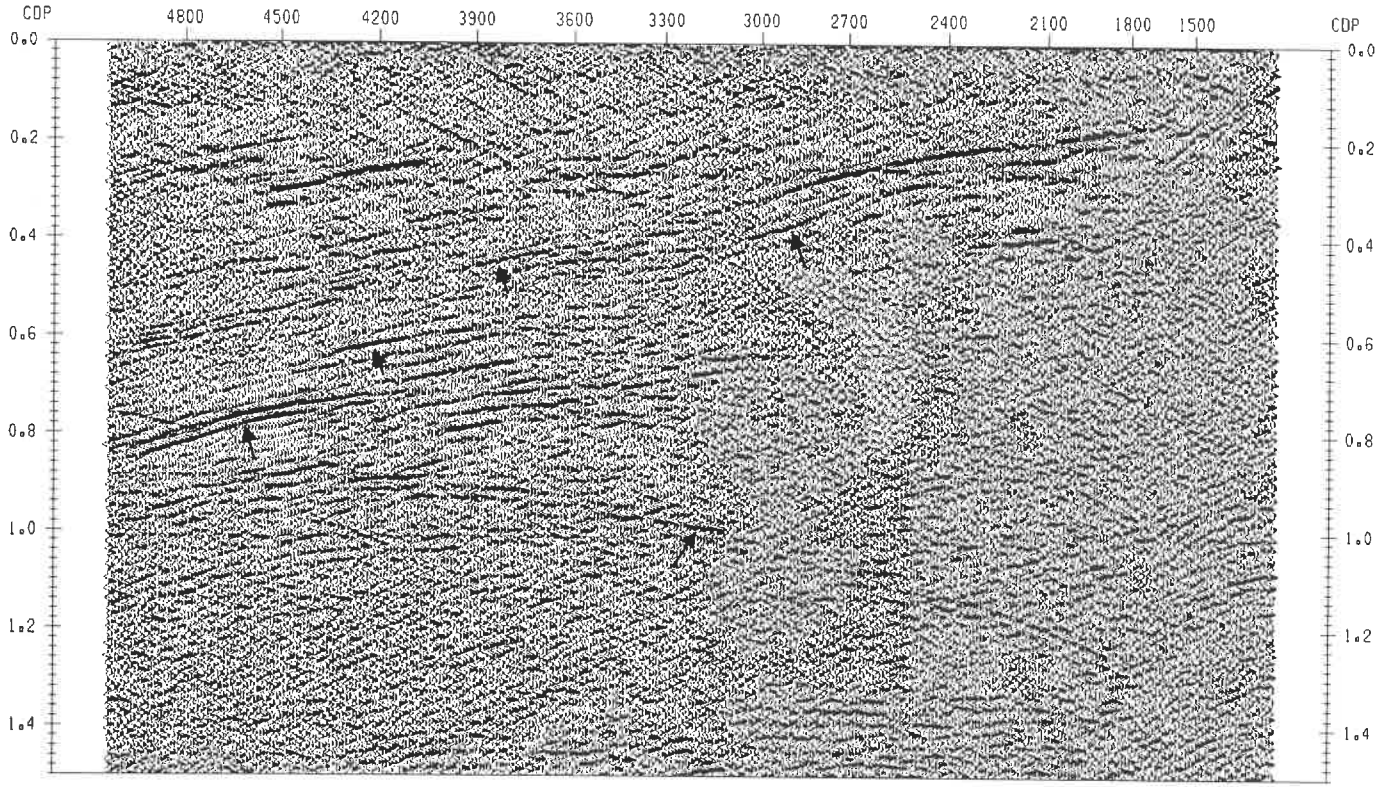

Figure 3.14b Line 29-3 after the crossdip corrections.

These residual statics are, therefore, usually estimated by statistical methods.

In the ITA software, there are a few modules for calculating residual statics. The super-fold module, which is based on the Ronen-Claerbout algorithm, is most commonly used. The basic idea behind the Ronen-Claerbout method is that the static shifts are determined so that the power in the final stack is maximized, i.e. the objective function is the power of CMP stack. To find the best static model, we can in principle try all possible models and choose the one that yields the best stack. In practice, however, for a single shot and receiver, stack and sum squares of the stack, we choose the static shift which gave the highest power. The algorithm builds a super-trace from all the traces of the shot profile in sequence, and then crosscorrelates this super trace with another super trace of all the traces in the relevant part of the stack in sequence without the contribution of that shot. The amplitude maximum of that crosscorrelation is then picked and the corresponding time shift stored (Ronen et al. 1985).

To estimate a shot-consistent static shift, the shot profile is crosscorrelated with the relevant part of the stack and the maximum is picked. The stack is corrected accordingly. The procedure is repeated until convergence is obtained (usually repeat 5 to 20 iterations):

Repeat { for every shot and every geophone, {

1) form the super traces;

2) crosscorrelate them;

3) pick the maximum;

4) correct the stack;

} constrain the statics (optional);

} until convergence expected.

The super-fold algorithm in INSIGHT calculates iteratively surface-consistent residual statics. It works best if an AGC has been applied and the data are sorted to the CMP domain. Also a velocity function as good as possible is needed for the NMO correction applied prior to running residual statics.

Residual statics produce good results on Line 29-3. Figure 3.15(a) is the CDP stack of this line between 3300CDP and 5300CDP with only elevation and refraction statics. The NMO velocities ware obtained by constant velocity analysis: stacking with different velocities (e.g. 5800 m/s, 5900 m/s, 6000 m/s, 6100 m/s, 6200 m/s, 6300 m/s, 6400 m/s), then picking the velocity which yields the best stack of a reflector. Because with a large time window the computation size will increase rapidly, and other events in that window will influence the crosscorrelation, it is a good idea to set different time windows for different segments in a CMP stacked section. Each window covers one reflector or a part of dipping reflector. In the situation of Line 29-3, two time windows were applied separately: firstly residual statics were applied on 0.05 to 0.55 s. then applied on 0.5 to 1.5 s. Both windows produced good convergence after 5 iterations. The total residual statics range from -6 ms to +6 ms (figure 3.8(c) and (d)) for receivers and shots. Figure 3.15 (b) is the stacked section after residual

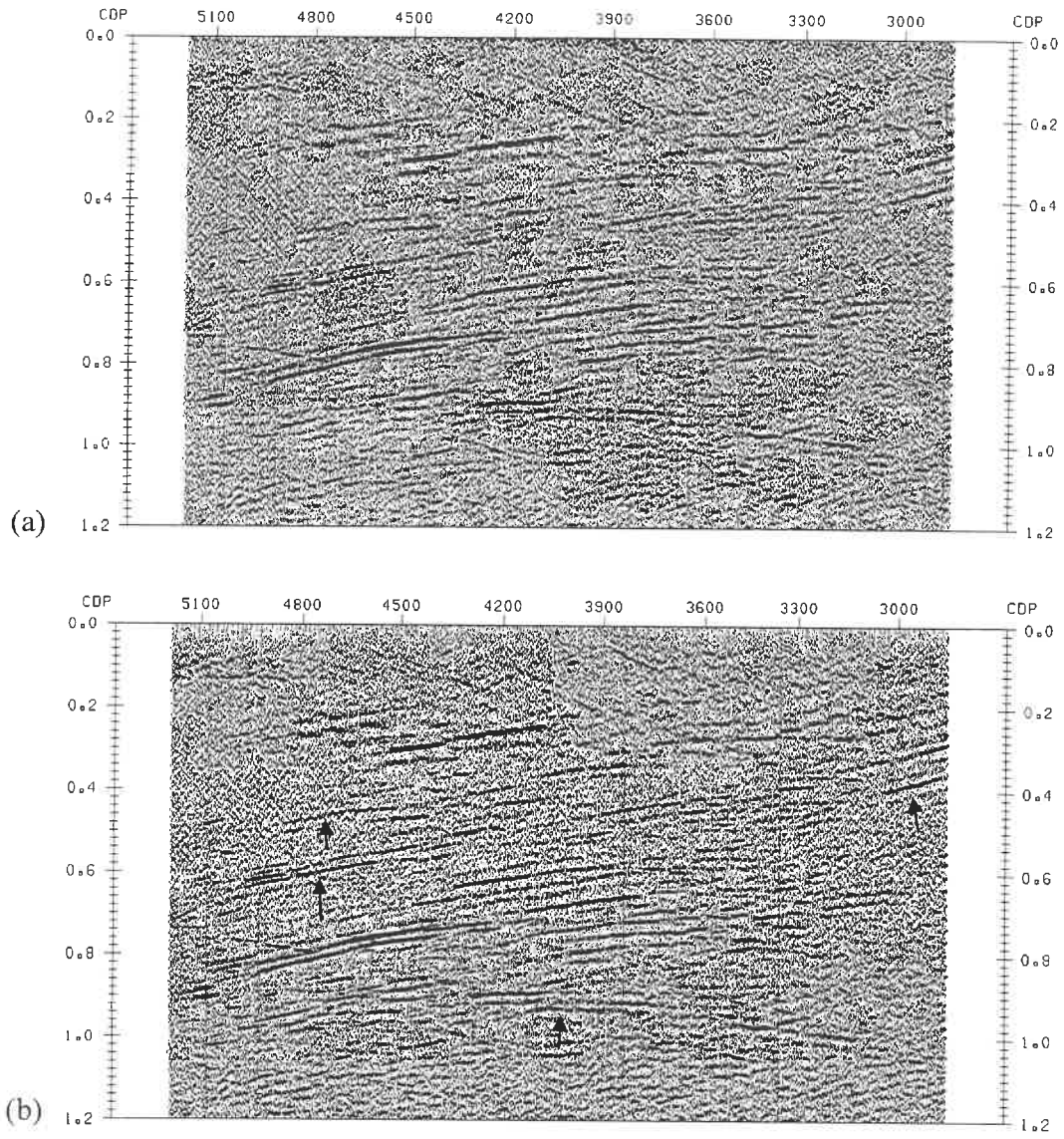

Figure 3.15 The effect of residual statics on a part of Line 29-3. (a) without residual corrections; (b) with residual corrections.

statics correction. The most improved structures are between 0.4 s and 1.2 s.

According to the theory of the Ronen-Clearbout method, this algorithm should be sensitive to errors in velocities. So the residual statics and the velocity analysis are usually iteratively applied several times to obtain an improved stack quality. Two iterations were applied to Line 29-3; however, no obvious changes were observed. Hence, a residual statics with the NMO velocities obtained above is enough for Line 29-3.

Residual statics is also necessary for Line93A. Constant velocity analysis (CVA) (3.4.7) is applied to produce good NMO velocities before operating residual statics. Two windows were applied. The first one was applied on the whole line (0.05 to 1.9 s). The second one was focused on the portion of interest (0.05 to 0.6 s). Both of them had 5 iterations. Figure 3.16 shows that the stack quality of Line 93A is improved in terms of the amplitude and continuity of reflectors.

3.4.7 Velocity Analysis

Given hyperbolic reflection events from layers in the earth, our objective is to combine the traces from various offsets in the CMP gather into a single high quality trace. If we know the stacking velocity of the reflection, we may apply NMO time corrections which depend on velocity, offset and two-way time to bring the reflection to the zero-offset arrival time so that

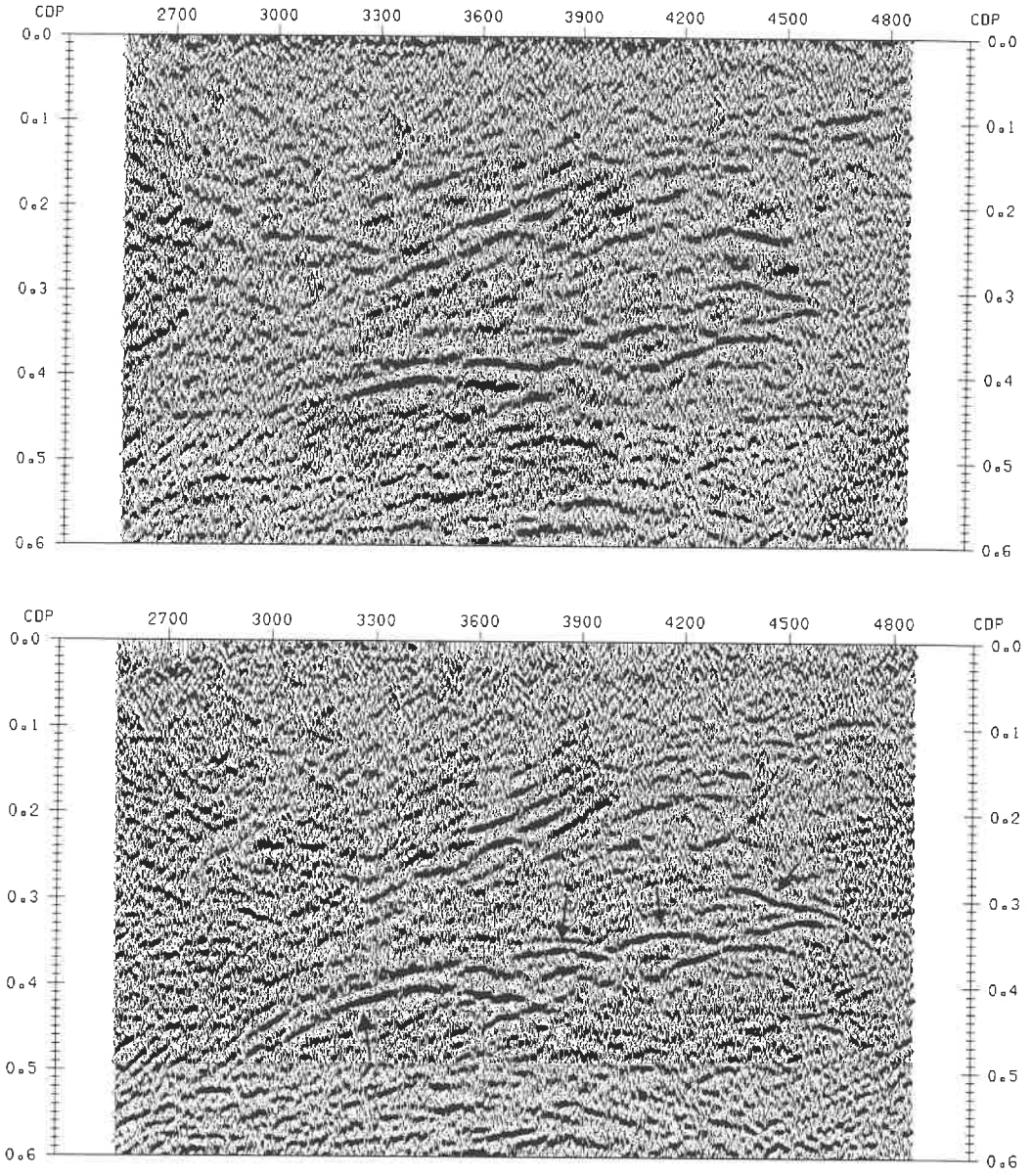

Figure 3.16 The effect of residual statics on the 2600-4850 CDPs of Line 93a.
Above: without residual corrections; Below: with residual corrections.

the reflection is aligned in the traces of a CMP gather before stacking. A precise velocity function is critical for a good quality final stack section.

There are several methods for velocity analysis. The technique of constant velocity analysis (CVA) is often appropriate in areas with complex structure. The basic idea of the CVA method is that stacking velocities are estimated from data stacked with a range of constant velocities on the basis of stacked event amplitude and continuity. A portion of a line (e.g. 24 CMPs, but perhaps entire line) are NMO-corrected and stacked with a range of constant velocity values. The results are displayed as panels. Stacking velocities are picked directly from the constant-velocity stack panel by choosing the velocity that yields the best stack response at a selected time. Two issues should be considered when applying the CVA method: (1) the range of velocities needed to stack the data. It should include all possible stacking velocities; (2) the spacing between trial stacking velocities. It should be small enough to obtain the best stack. The velocities obtained from the CVA technique are the best stacking velocities, but may not be representative of actual subsurface velovities.

For Line 29-3, a range of constant velocity values between 5000.0m/s and 7000.0m/s, increasing by 100.0 m/s were used. A 20-CMP-gather is chosen for the stack panel. 11 different CMP locations are analyzed, and in total 61 velocity functions (velocity as the two-way travel time and CMP function) are obtained.

3.4.8 DMO (dip moveout)

DMO, dip moveout, is a special process for enhancing dipping events in seismic data processing. It can be viewed both geometrically and in term of the NMO equation.

It is well known that common-midpoint gathers (CMP) do not contain reflections with common reflection points (CRPs), or common depth points (CDPs), when reflectors are dipping. The displacement L between them is given by (Levin, 1971):

$$L = \frac{h^2}{D}\cos\theta\sin\theta \qquad (3.3)$$

where h is half the source-receiver offset; D is the vertical distance from the midpoint to the reflector; θ is the reflector dip. To compensate for this reflection point displacement, DMO must move the non-zero-offset reflection a distance L (in the up dip direction) so that it will be stacked with a zero-offset reflection having the same reflection point.

From the NMO equation, we also can see why DMO is required for a dipping event. For a CMP with a single dipping reflection, the NMO equation (Levin, 1971) is :

$$t^2(x) = t^2(0) + \frac{x^2\cos^2\theta}{v^2} \qquad (3.4)$$

where θ is the reflector dip, v is the medium velocity above the reflector, and x is the source-receiver separation. This equation can be rewritten as :

$$t^2(x) = t^2(0) + \frac{x^2}{V^2} - \frac{x^2 \sin^2\theta}{v^2} \qquad (3.5)$$

The second term of the equation (3.5) is related to the conventional NMO, while the third part of it is associated with dip moveout (DMO). This equation implies that for a quality stack section, we must apply a NMO correction as well as a DMO correction.

DMO is a partial prestack migration process. Compared to full prestack migration, DMO operates on a limited offset range and requires less computing time. NMO + DMO + stack + time migration after stack is approximately equivalent to time migration before stack.

From the equation (3.5), we can see that DMO acts greater at shallower depth and larger offset. In fact, it does nothing to the zero-offset section. Also, the steeper the event, the greater the effect of DMO; flat events remain unaltered.

A typical DMO processing flowchart is:

field data
⇓
velocity analysis
⇓
NMO using flat-event velocities
⇓
DMO correction
⇓
remove initial NMO
⇓
perform velocity analysis

⇓
NMO correction using new velocities
⇓
stack to zero offset

The theoretically correct NMO velocity before DMO is the zero dip (flat-event) stacking velocity. This avoids the NMO being contaminated by dip variation (Deregowski and Rocca, 1981). An average constant velocity is a good choice for this purpose. However, if a velocity analysis is applied before NMO, it can be used but all analysis from CMPs in areas of steep dip should be edited out. After applying DMO, the initial NMO function is removed and a standard velocity analysis performed. The new velocities will usually be smaller than the old ones. When the new velocities reveal large differences from the initial NMO, an iterative loop may be applied.

Both Line 29-3 and Line 93a contain several dipping events. With conventional seismic processing, these dipping events are poorly stacked. To overcome this difficulty, DMO-processing is necessary. The average velocity of 6000 m/s was used for NMO before DMO. Figure 3.17 highlights the effects of DMO-processing on Line 93a. Although DMO does correct dipping events and produce a better stacked section, reflectors are not migrated to their true subsurface positions, unlike the prestack time migration. Therefore, a subsequent application of post-stack migration is required.

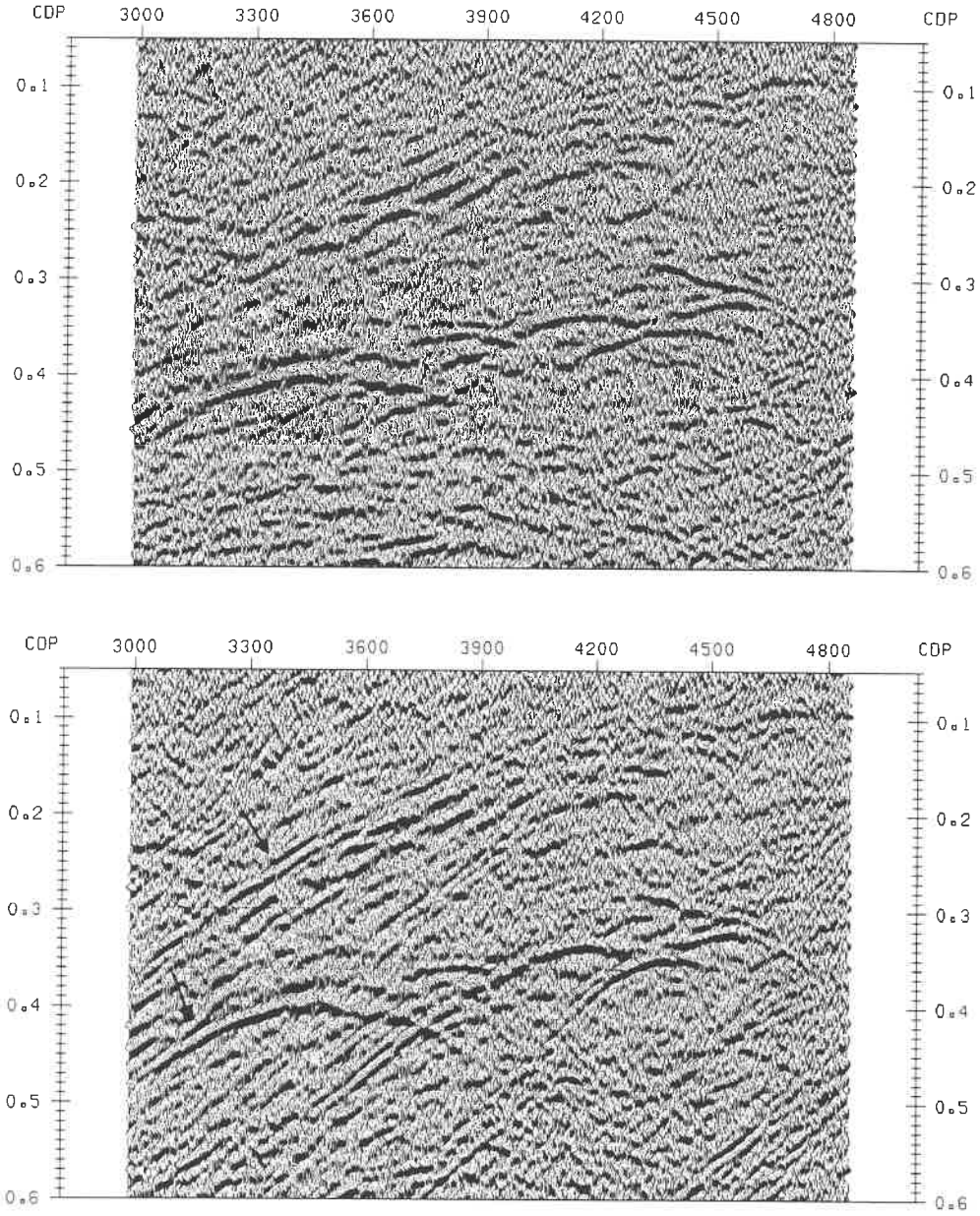

Figure 3.17 The effect of DMO on a part of Line 93a. Above: without DMO; Below: with DMO.

3.4.9 Migration

The section obtained from a stack is assumed to represent a zero-offset section, i.e: the section that would be recorded if both source and receiver were coincident. However, for any reflector that is not horizontal, the apparent subsurface location will not correspond to the true subsurface position. Migration of seismic data moves dipping reflections to their true subsurface location. In addition, migration also collapses diffractions that are associated with faults, truncated reflectors etc..

Migration can be done either in the time domain or in the depth domain. As long as lateral velocity variations are mild, a time migration, which produces a migrated time section, can be applied. However, when the lateral velocity gradients are large, a depth migration, the output of which is a depth section, must be applied instead of time migration.

No current migration technique handles all of the difficulties of noise, rapidly varying velocities, steep dips, and other problems perfectly. Techniques vary greatly in performance relative to these problems. Three of the major techniques of migration are: diffraction (Kirchhoff) migration, finite-difference migration, and frequency domain (f-k) migration. Frequency domain migration is used for migration of Line 29-3 migration. The advantages of this method include fast computation time and excellent performance for steep dip. Disadvantages include difficulties with widely varying velocity functions. Fortunately, this

condition does not apply to Line 29-3 and Line 93a.

The theory of the frequency domain migration is based on straightforward geometric techniques and simple frequency domain observations (Chun, 1981). In the time section, the angles of a single reflector before and after migration have the relationship:

$$\tan\theta_m = \frac{\tan\theta}{\sqrt{1-(\frac{v}{2})^2 \tan\theta}} \qquad (3.6)$$

where θ_m is the migrated angle; θ is the unmigrated angle; V is the velocity. Also, the displacement $d = (d_x , d_t)$ of a point P are effected by migration as:

$$d_x = V^2 T \frac{\tan\theta}{4} \qquad (3.7)$$

$$d_t = T \left[1-\sqrt{1-(\frac{V}{2}\tan\theta)^2}\ \right] \qquad (3.8)$$

where V is the velocity; T is the two time; θ is the unmigrated angle. These formulae show that both the migrated dip angle and the migrated displacements depend on not only the original dip angle, but also the velocity of migration. Migration with a nonconstant velocity is a delicate and complicated problem in itself. But, here the simple approximation using smoothed stacking velocities did a reasonable job.

After the Fourier transform to the frequency domain, no matter where they are located in space, all events of the same dip appear along lines normal to that dip. Thus, events of the same dip can be migrated together, that is: all the scattered dipping events in the depth domain are handled easily in the frequency domain. This is the good reason why migration are applied in the frequency domain. Using the Fourier transform every event on a seismic section may be considered as a sum of events of a single dip and the section a sum of all of such events. The entire migration process may be viewed as the simple procedure applying the equations (3.6) (3.7) and (3.8) to a vast sum of simple events.

Figure 3.19 is the migrated section of Line 29-3 using frequency domain migration with a smoothed velocity 6000 m/s applied to constant offset gathers after DMO. After f-k migration and sort to CDP gather, a semblance velocity analysis was applied to obtain revised stacking velocities. Then NMO and stack were applied with the new velocities. Comparing with the unmigrated section (figure 3.18), dip reflectors become steeper, shorter and are moved in the updip direction. The performance of the migration is not bad at all on this section.

The same migration procedure was applied on Line 93A. Figure 3.20 is the unmigrated section of Line 93A, while figure 3.21 is the f-k migrated one. Except the reflectors becoming shorter, steeper and being moved to the updip direction, the bow-ties (beneath CDP 3000 to 4700 between 0.2 s and 0.5 s) were opened by the migration.

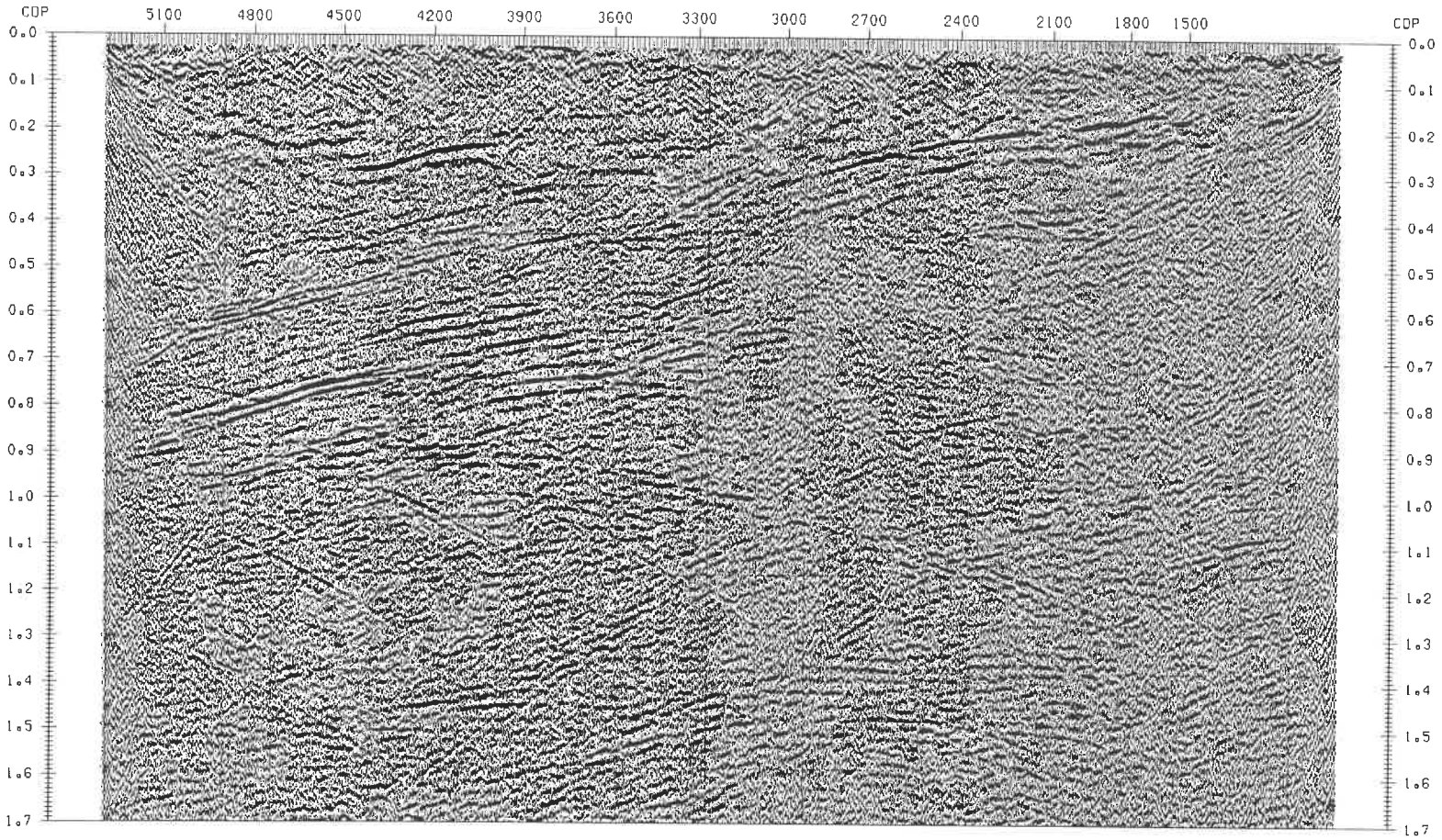

Figure 3.18 The unmigrated stack section of Line 29-3.

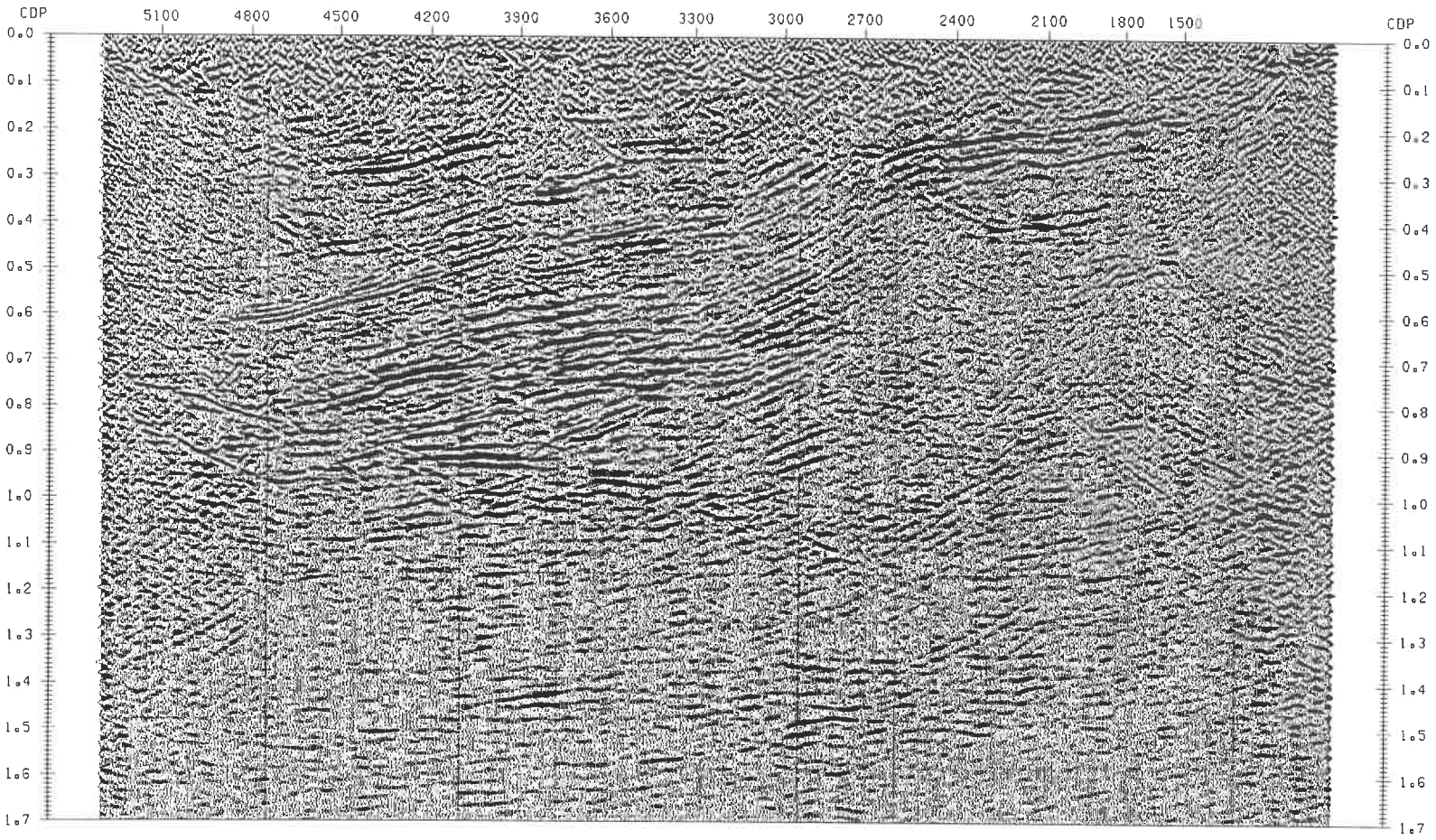

Figure 3.19 The migrated stack section of Line 29-3.

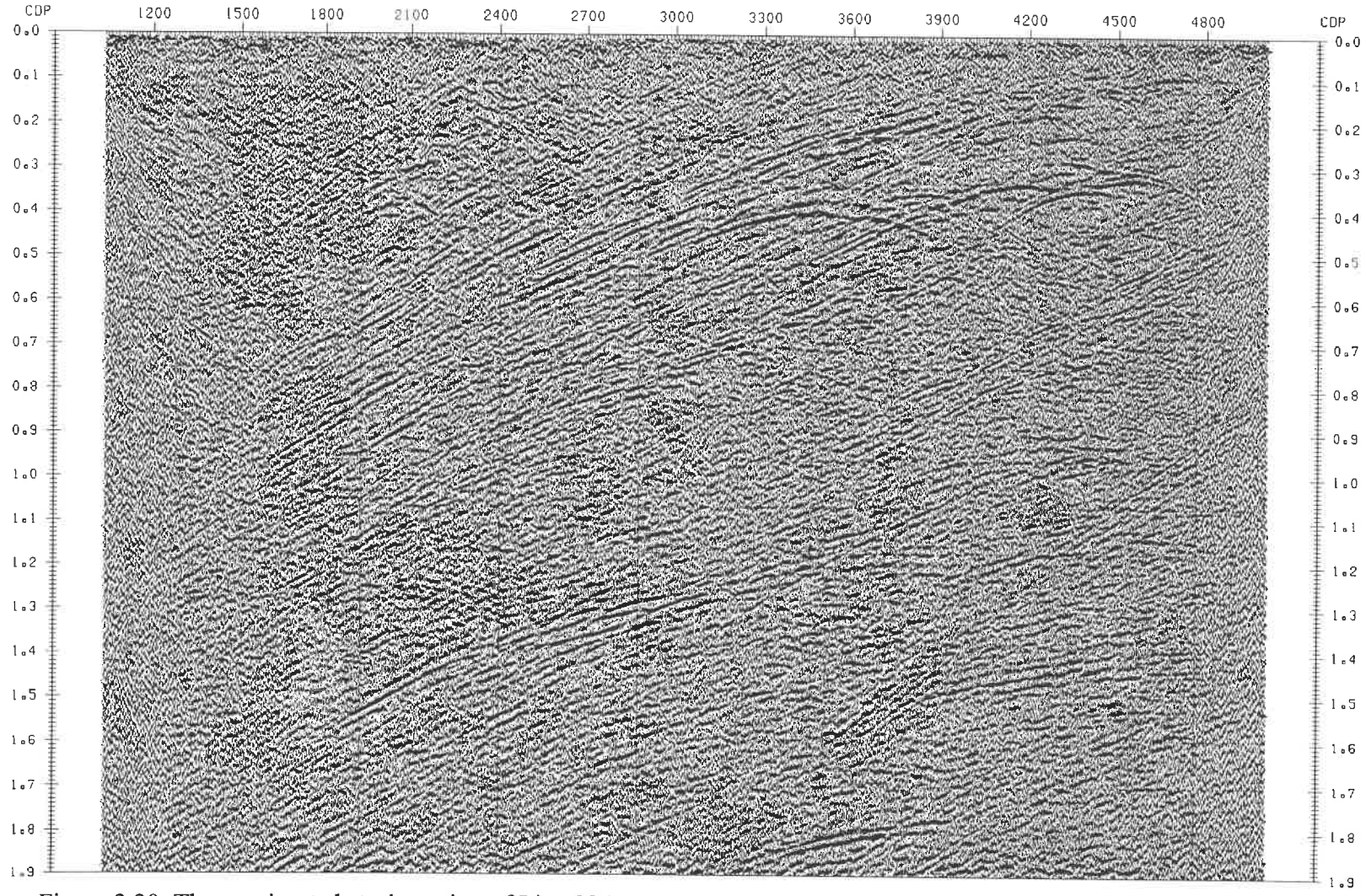

Figure 3.20 The unmigrated stack section of Line 93A.

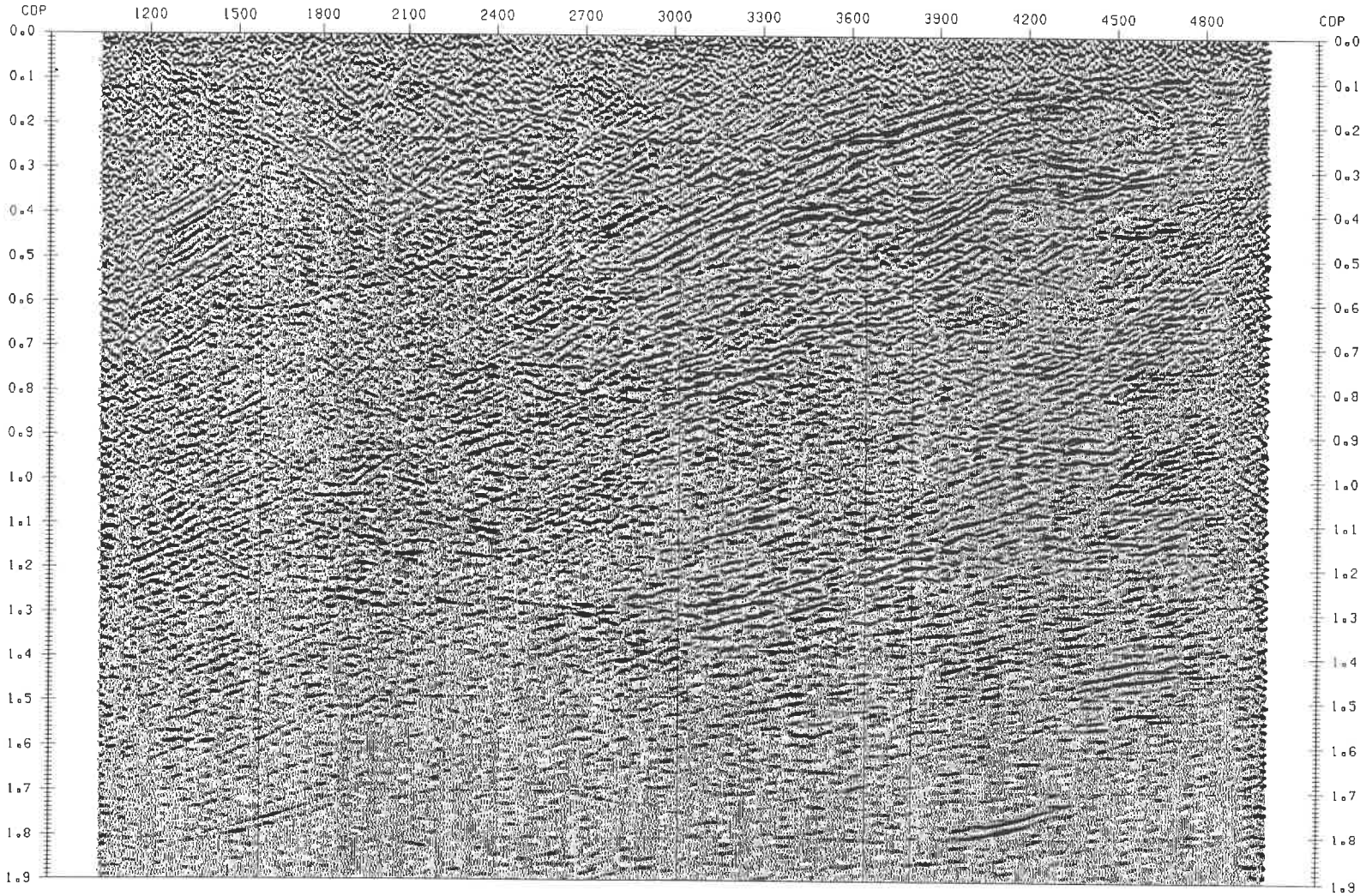

Figure 3.21 The migrated stack section of Line 93A.

3.5 Interpretation of seismic profiles Line29-3 and Line93A

Since the two high frequency seismic profiles Line 29-3 and Line 93A intersect and two boreholes B2 and B4 provide good geological control, a precise interpretation of this area is possible.

3.5.1 The interpretation of Line 29-3

The interpreted section of the Line 29-3 is shown in figure 3.22. The section was DMO processed and followed by post-stack migration, so the reflections on this section have a better representation of the true attitude and position of subsurface reflectors. Two boreholes located on the eastern portion of the line provide good stratigraphic control for the interpretation.

The east part of the seismic line, between CDP 950 and 2700, is characterized by a sequence of strong, west-dipping reflections overlain by a seismically transparent zone. The reflective sequence originates from interlayered basalt, gabbro, rhyolite and tuffite. It clearly defines the lower Wabassee Group. The detailed reflectors within the reflective sequence are difficult to identify. The overlying upper Wabassee Group seems non-reflective. The Key Tuffite and the underlying Watson Lake Group are characterized by their low reflectivity and can be identified at the base of the lower Wabassee Group. The Watson Lake Group appears also

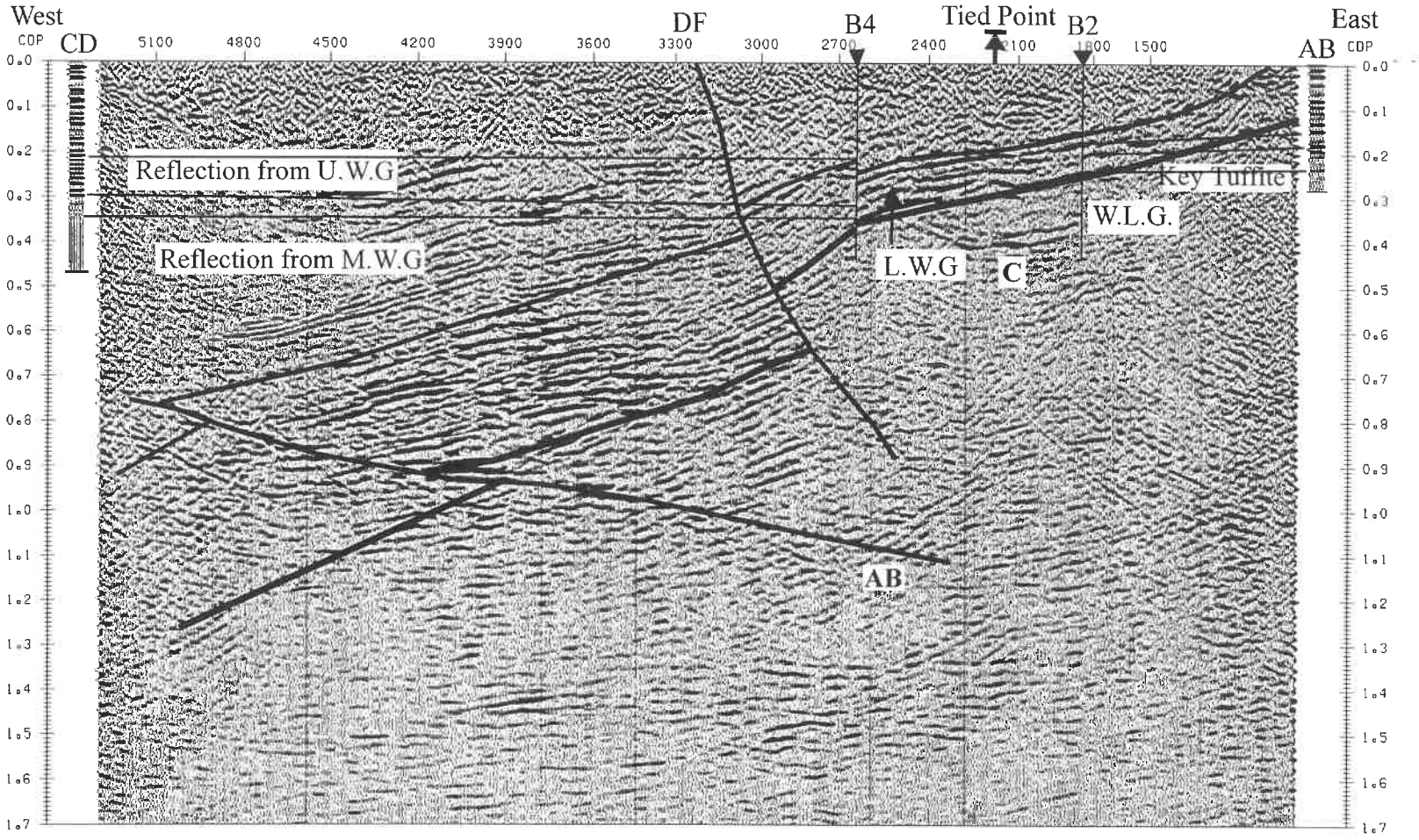

Figure 3.22 Interpretation of main features of Line 29-3. (W.L.G.: Watson Lake Group; L.W.G.: Lower Wabassee Group; M.W.G.: Middle Wabassee Group; U.W.G.: Upper Wabassee Group; AB: the synthetic seismogram from B2; CD: the sonic seismogram from B4.)

non-reflective except the seismic amplitude anomaly (C) at about 0.4 s two-way-time (1200 m depth) beneath CDPs 1850 to 2350.

Two boreholes provide evidence for this interpretation. Hole B2 is 758 m deep and intersects the Key Tuffite at a depth 685 m. Hole B4 has a depth of 1442 m and it reaches the Key Tuffite at about 1291 m (Adam et al., 1993). A density logging study was conducted in hole B2 and full waveform sonic logs were recorded at 10cm interval in both holes. P-wave velocities are obtained from the full waveform sonic logs by calculating the traveltime difference between near and far receivers (the distance between the near and far receivers is one foot). The seismic velocities for these hole surveys range from less than 6 to 7 km/s in some gabbros. Figure 3.23 and figure 3.24 show the borehole results from B2 and B4, respectively. the Key Tuffite contains some sulphide, so it is easily recognized by the high densities, but its velocity is not reduced significantly. The top of the lower Wabassee Group is associated with a basalt-gabbro sequence, which has a higher velocity, implying a higher impedance and seismic reflective coefficient. The Watson Group consists of rhyolites, characterized by reduced densities and velocities (low seismic reflection coefficients). These measurements correlate well with the prominent reflections on the seismic profile.

The Daniel fault (DF) lies beneath CDP 2900. The DF truncates the west-dipping reflections around CDP 2800 to 2900. The displacement between the east and west of DF of the lower Wabassee Group is about 0.2 s (TWT), i.e, 600 m. The DF is probably not a single fault but

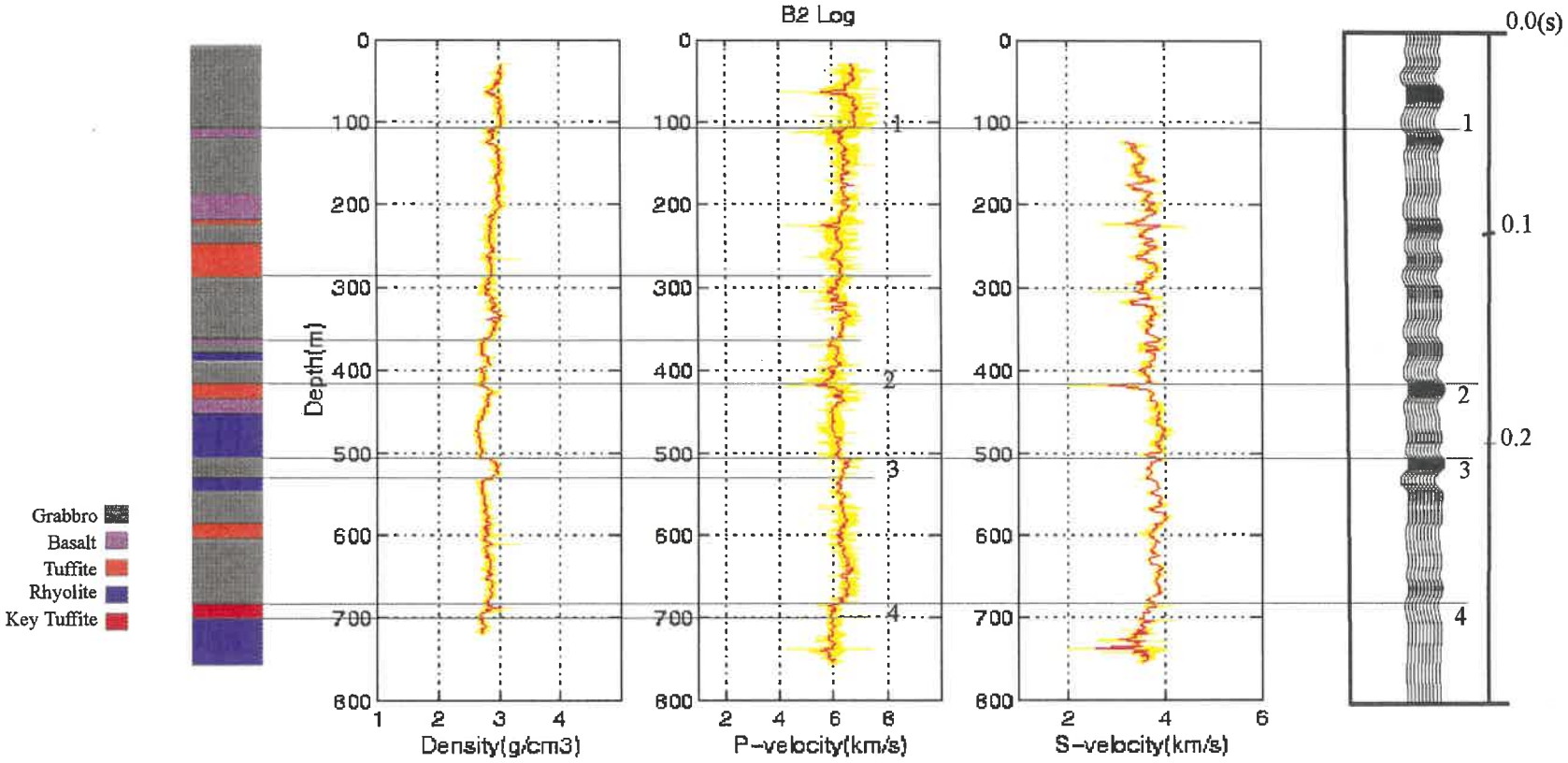

Figure 3.23 The lithology, density, P(S)-velocity and synthetic seismogram for B2. (Red Line: smoothed value).

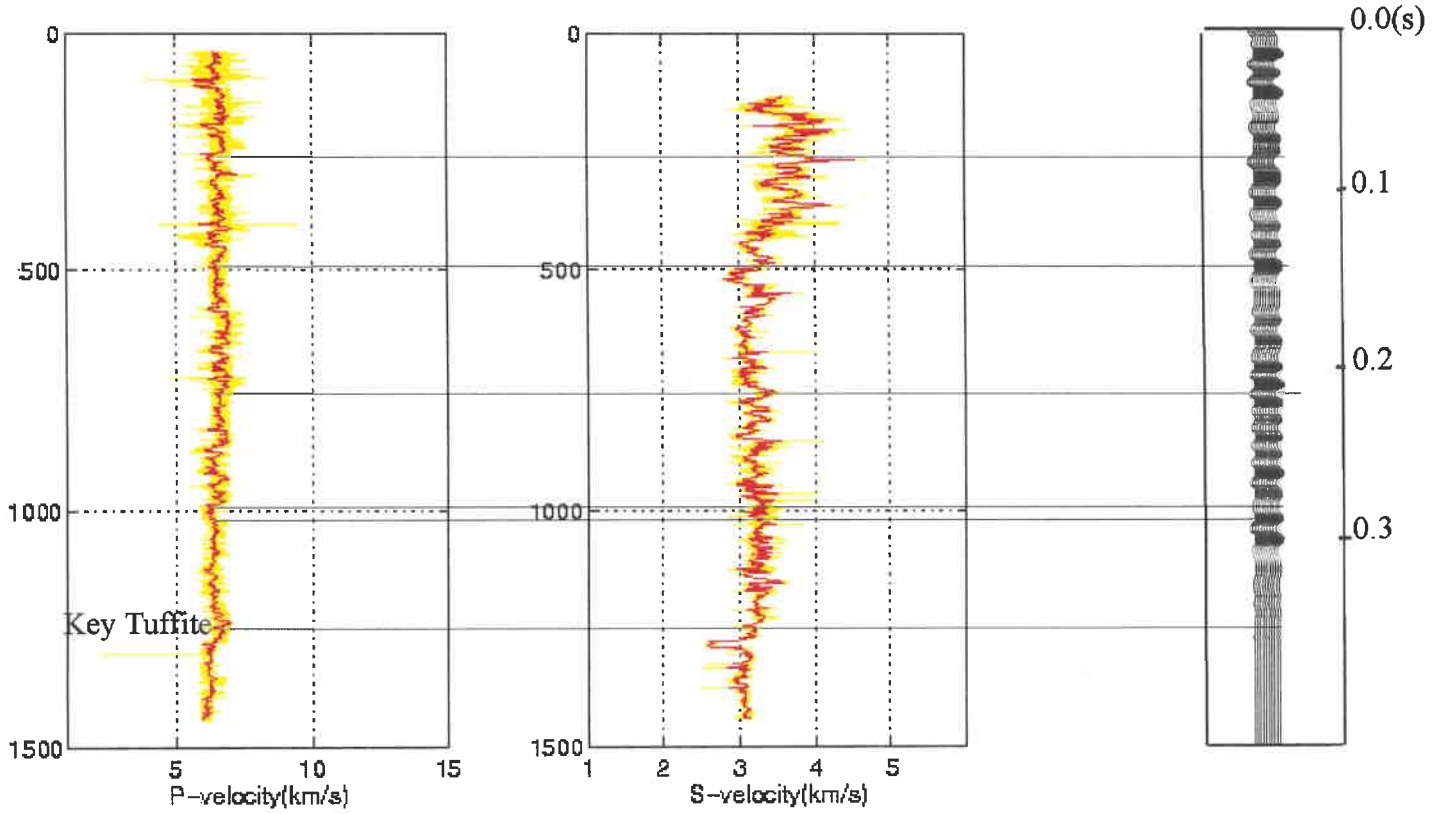

Figure 3.24 The P(S)-velocity and synthetic seismogram for B4. (Red Line: smoothed value).

rather a complex zone from the seismic image. The seismic reflection sequence within it seems to be down-faulted to the west.

The west part of Line 29-3 (CDP 3000 to 5300) is dominated by the west-dipping strong reflections associated with lower Wabassee Group. No borehole control is available. The reflective package can be traced to a depth of 3.6 km (1.3 TWT) at the end of the profile. The thickness of the lower Wabassee Group on this part is around 900 m.

There is only one major west-east-dipping reflection (AB) on the seismic section. It is beneath CDP 2900 to 5200 between 0.75 s and 1.1 s TWT, and probably is a thrusting fault.

3.5.2 The interpretation of Line 93A

An interpretation of the seismic profile Line 93A is presented in figure 3.25. The section was also DMO processed and post-stack migrated. Prominent south dipping reflections can be traced from the end north of the line to CDP 2700 on the stacked section. The tie point of Line 29-3 and Line 93A is station 392 (3920 CDP) on Line 93A, and station 220 (2200 CDP) on Line 29-3. At this point, a package of reflectivity around 0.12s thick can be identified between 0.15 s and 0.27 s recording time (TWT) on both lines. This reflective package corresponds to the gabbro-rhyolite boundary along with the Key Tuffite in the borehole logs. The synthetic seismograms calculated from density (taking a constant for B4) and P-wave

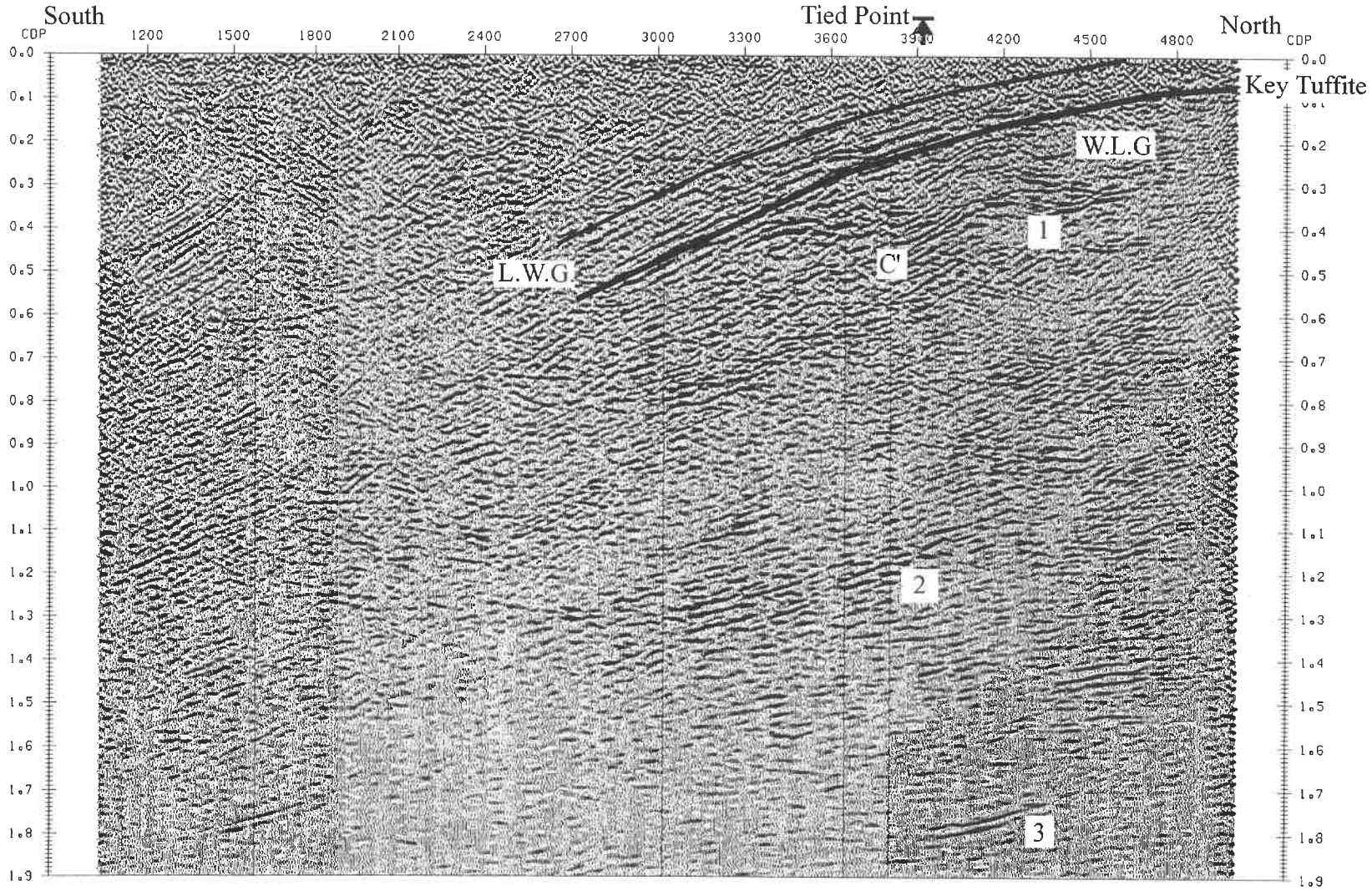

Figure 3.25 Interpretation of main features of Line 93A. (L.W.G.: Lower Wabassee Group; 1: Reflections from Watson Lake Group; 2, 3: reflections from deep structures; W.L.G.: Watson Lake Group.)

velocity logs, using a band limited wavelet (30-120 Hz), correlate well with the surface seismic reflection data. Hence, these three data sets (Line 29-3, Line 93A, boreholes) are in good agreement with each other (figure 3.26).

The reflection C' on the section 93A (figure 3.25) correlates with C on the section Line 29-3 (figure 3.22). It occurs between 0.36 and 0.42 s on both lines. There are strong reflections beneath CDP 3000 to 4700 between 0.27 and 0.43 s. They are from Watson Lake Group. The deeper reflections are also probably associated with the Watson Lake Group.

The reflections from the lower Wabassee Group and the Watson Lake Group have a of dip around 30^0 towards the south of Line 93A. There are no major breaks in the continuity of these reflections, but a few small breaks do exist at shallow times beneath CDP 4300 to 4900, which are probably caused by the first break muting.

The Daniel fault should be reflected on Line 93A as north-dipping reflections, but they are not apparent. The south-dipping reflections increase beneath CDP 3000 to 4200. There is a strong reflection under CDP 3800 to 4300 at 1.75 s.

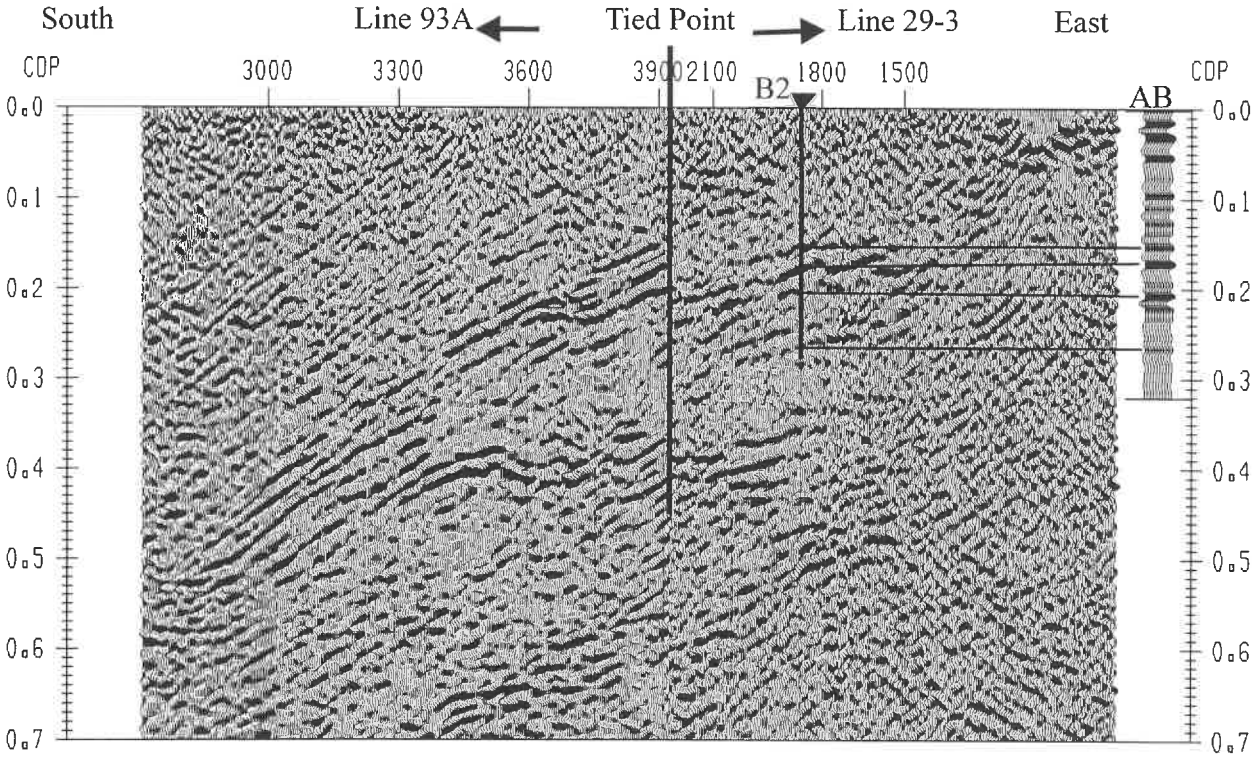

Figure 3.26 Interpretation of Line 29-3, Line 93A and borehole B2. (AB: the synthetic seismogram of B2.)

CONCLUSION

Vertical seismic profiling (VSP) is a measurement procedure in which a seismic signal is generated at the surface of the earth and is recorded by geophones located at various depths of a drilled well. VSP surveys are one of the most accurate methods of determining seismic velocity. The major difference of VSP data processing from traditional seismic reflection data processing is the separation of upgoing waves (reflection waves) from downgoing waves (direct waves). Several numerical techniques can be used for this purpose. The data processing of the Matagami VSP includes: time correction to assure that the differences between start-recording time and shot-time for all geophones are the same; noise analysis to remove noise generated from active mining camps; and downgoing and upgoing wave separation to achieve the useful reflection information. However, the upgoing waves are so weak that the downgoing waves are still very strong on the final section.

The reprocessing of Line 29-3 successfully mapped a portion of the Matagami mining camp. Accurate refraction statics corrections and crossdip corrections made greatest the contribution to the improved quality of the stack section comparing with the LITHOPROBE report. Table 3.4 summaries the reprocessing parameters. The final stacked section confirms: the Wabassee Group is characterized by continuous prominent reflections and the Watson Lake Group is almost non-reflective. The lower Wabassee Group may be used as a marker to define indirectly the Key Tuffite, located at the contact between the Watson Lake and the

Wabassee Groups. The seismic reflection data also show the location and attitude of the Daniel fault zone. A possible thrusting fault in the west-east direction can be observed on the deep section. The two available borehole data sets closing to Line 29-3 provide important geological constraints.

Data reprocessing of Line 93A includes geometry, first break muting and shear wave removal. Significant improvement of the final stacked section is achieved by carefully correcting for refraction statics, surface consistent residual statics and DMO (table 3.5). The reflective package originating from the lower Wabassee Group on Line 93A corresponds well to the reflections on Line 29-3. On the final stacked section of Line 93A, not only can reflection from the Wabassee Group be observed, but the deep reflections associated with the Watson Lake Group can be also seen. It is possible to identify several breaks in the continuity of the reflections above the Watson Lake Group, which may be due to faulting of this sequence.

The success of the interpretation of two high resolution seismic reflection profiles provides us with an evidence of the application of seismic methods for mineral exploration purposes.

Table 3.4 Data Reprocessing Sequence of Line 29-3

BASIC PROCESSING	
Crooked Line Geometry	
Noise Analysis	45, 60, 120 Hz noise removal
Bandpass Filter	20/30-100/120 Hz
Scale	200 ms AGC
First Break Muting	
first break analysis	FB picking for each shot
Shear Wave Removal	
Refraction Statics	Datum 300 m above sea level; replacement velocity = 6 km/s
Stacking Velocity Analysis	Based on stacking quality with different velocity
ADVANCED PROCESSING	
Crossdip Analysis	
CDP Residual Statics	window 50 - 550 ms, 500 - 1500 ms maximum shift allowed 40 ms
Dip Moveout (DMO)	CDP bin size 80 m
Stacking Velocity Analysis	20-CMP gather, every 80 CDP
DISPLAY	
F-K Migration	6000 m/s velocity
UNMO	
Bandpass Filter	25/30--100/120 Hz
Velocity Analysis	
NMO	
Stack	

Table 3.5 Data Reprocessing Sequence of Line 93A

BASIC PROCESSING	
Geometry	
Noise Analysis	45, 60, 120 Hz noise removal
Bandpass Filter	20/30 - 100/120 Hz
Scale	200 ms AGC
First Break Analysis and Muting	
Shear Wave Removing	
Refraction Statics	Datum 300 m above sea level, Replacement velocity = 6 km/s
ADVANCED PROCESSING	
CDP Residual Statics	window 50-1900 ms, 0.05-0.6 s; max-shift allowed = 40 ms
Dip Moveout	CDP bin size 80 m
Stacking Velocity Analysis	20-CMP gather for every 80 CDP
DISPLAY	
F-K migration	6000 m/s velocity
UNMO	
Bandpass Filter	25/30-100/120 Hz
Velocity Analysis	
NMO	
Stack	

REFERENCES

ADAM, E. and MILKEREIT, B. Physical rock property studies along LITHEPROBE seismic profile 29-3, Matagami: Geological Survey of Canada, Continental Geoscience Division, 1 Observatory Crescent, Ottawa.

ADAM, E. and LANGLOIS, P. (1995) Elimination of monofrequency noise from seismic records: Ecole Polytechnique, Dépt. de Génie Minéral.

ADAM, E., MILKEREIT, B., BARNES, A., BEAUDRY., C., PINEAULT, R., MARESCHAL, M., and CINQ-MARS., A. (1992) Results from LITHOPROBE seismic reflection profiling in the Matagami Area, Abitibi Melt, Quebec: 38 AG LITHOPROBE WORKSHOP.

BARNES, A.E., BELLEFLEUR, G., LUDDEN, J.N. and MILKEREIT, B. (1994) Appraisal of the parameters of the LITHOPROBE Abitibi-Grenville seismic reflection survey: Geoscience Canada, 21, 49-57.

BEAUDRY, C. and GAUCHER, E. (1986) Cartographie géologique dans la région de Matagami. Ministère de l'Energie et des Ressources du Québec, Report MB 86-32.

CHUN, J.H., and JACEWITZ, C.A., (1981), Fundamentals of frequency domain migration: Geophysics, 46, 717-733.

CHARTRAND, F. and CATTALANI, S. (1990) Massive sulphide deposits in Northwestern Quebec: In the Northwestern Quebec Polymetallic Belt. Edited by M. Rive, P. Verpaelst, Y. Gagnon, J.M.Lulin, G.Riverin, and A.Simard. Canadian Institute of Mining and Metallurgy, Special Volume 43, 77-91.

COPPENS, F. (1985) First arrival picking on common-offset trace collections for automatic estimation of static corrections: Geophys. Prosp., 33, 1212-1236.

DEREGOWSKI, S. and ROCCA, F. (1981) Geometrical optics and wave theory for constant-offset sections in layered media: Geophys. Prosp., 29, 374-387.

DUMAS, I.. (1995) Interprétation de la ligne régionale 21 de sismique réflexion dans le groupe de blake river, Abitibi, Quebec: Thesis of Master, département de génie minéral, Ecole Polytechnique de Montreal.

GREEN, A.G., MILKEREIT, B., MAYRAND, L.J., LUDDEN, J.N., HUBERT. C., JACKSON, C.L., SUTCLIFFE, R.H., WEST, G.F., and VERPAELST, P., (1990), Deep structure of an Archean greenstone terrane: Nature, Vol 344, 327-330.

HAGEDOORN, J.G. (1959) The plus-minus method of interpreting seismic refraction sections: Geophys. Prosp., 7, 158-182.

HAMPSON, D., and RUSSELL, B. (1984) First-break interpretation using generalized linear inversion: Journal of the Canadian of Exploration Geophysicists, 20, No.2, 40-45.

HARDAGE, B.A. (1985) Vertical Seismic Profiling, Part A: Principles, 2nd edition, Seismic Exploration, Geophysical Press, 509 p.

JACKSON, S.L., CRUDEN, A.R., WHITE, D., MILKEREIT, B. (1995) A seismic-reflection-based regional cross section of the southern Abitibi greenstone belt: Can. J. Earth Sci., 32, 135-148.

LARNER, K.L., GIBSON, B.R., CHAMBERS, R., and WIGGINS, R.A. (1979) Simultaneous estimation of residual statics and crossdip corrections: Geophysics, 44, No.7, (July 1979), 1175-1192.

LEVIN, F.K. (1971) Apparent velocity from dipping interface reflections: Geophysics, 36, 510-516.

MILKEREIT, B., ADAM, E., BARNES, A., BEAUDRY, C., PINEAULT, R., and

CINQ-MARS, A. (1992) An application of reflection seismology to mineral exploration in the Matagami area, Abitibi Belt, Quebec; in current research, Part C; Geological Survey of Canada, Paper 92-1C, 13-18.

MILKEREIT, B., WHITE, D., ADAM, E., BELLEFLEUR, G., CALVERT, A. (1994) Preliminary Progress Report for 1993 Lithoprobe Seismic Surveys at Matagami.

MILKEREIT, B. and ADAM, E. (1994) Reflection Seismic Profiling across the Matagami Mining Camp.

PERZ, M. and WANG, W. (1992) Refraction statics using 'refstat': LSPF Newsletter, 5.2, 33-40.

PICHE, M., GUHA, J., GAIGNEAULT, R., SULLIVAN, J.R., and BOUCHARD, G. (1990) Les gisements volcanogènes du camp miner de Matagami: structure, stratigraphie et implications métallogéniques: in: The Northwestern Quebec Polymetallic Belt: edited by M. Rive, P. Verpaelst, Y. Gagnon, J.M. Lulin, G. Riverin, and A. Simard; The Canadian Institute of Mining and Metallurgy, Special Volume 43, 327-335.

RONEN, J. and ClAERBOUT, J. F. (1985) Surface-consistent residual statics estimation by stack-power maximization: Geophysics, 50, No.12 (December 1985), 2759-2767.

SENESCHAL, G., MARESCHAL, M., HUBERT, C., CALVERT, A., GRANDIEAN, G., and LUDDEN, J. (1995) Integrated geophysical interpretation of crustal structures in the northern Abitibi Belt: constraints from seismic amplitude analysis.

SHERIFF, R. E. (1982) Exploration Seismology: History, Theory and Data Acquisition: Cambridge University Press, Cambridge, 253 p.

TELFORD, W. M., GELDART, L. P., SHERIFF, R. E. (1990) Applied geophysics, Cambridge Univeristy Press, Second Edition, 770 p.

YILMAZ, O. (1987) , Seismic Data Processing, Society of Exploration Geophysicists, 526 p.